Petroleum Science 21 (2024) 2005–2022

Contents lists available at ScienceDirect

Petroleum Science

journal homepage: www.keaipublishing.com/en/journals/petroleum-science

Original Paper

Hole cleaning evaluation and installation spacing optimization of cuttings bed remover in extended-reach drilling

Shuo Peng [a, b], Wen-Jun Huang [a, b, *], De-Li Gao [a, b, **]

[a] MOE Key Laboratory of Petroleum Engineering, China University of Petroleum-Beijing, Beijing, 102249, China
[b] State Key Laboratory of Petroleum Resources and Engineering, China University of Petroleum-Beijing, Beijing, 102249, China

ARTICLE INFO

Article history:
Received 24 April 2023
Received in revised form
12 March 2024
Accepted 12 March 2024
Available online 16 March 2024

Edited by Jia-Jia Fei

Keywords:
Extended-reach drilling
Drilling hydraulics
Cuttings transport
Hole cleaning
Cuttings bed remover

ABSTRACT

In extended-reach or long-horizontal drilling, cuttings usually deposit at the bottom of the annulus. Once cuttings accumulate to a certain thickness, complex problems such as excessive torque and drag, tubing buckling, and pipe stuck probably occur, which results in a lot of non-productive time and remedial operations. Cuttings bed remover can efficiently destroy deposited cuttings in time through hydraulic and mechanical stirring effects. This paper aims to build a method for hole cleaning evaluation and installation spacing optimization of cuttings bed remover to improve the wellbore cleaning effect. Firstly, a Computational Fluid Dynamics approach with Eulerian–Eulerian multiphase model was utilized to investigate the mechanism of cuttings transportation, and a new type of cuttings bed remover was designed. Next, an evaluation method of hole cleaning effect of remover was established. After that, the effects of several drilling parameters on hole cleaning including flow rate of drilling fluid, rotational speed of drillpipe, rate of penetration, wellbore size, rheological property of drilling fluid, and remover eccentricity on the performance of cuttings bed remover were investigated. The results demonstrate that the new type of remover with streamline blade performs better than conventional removers. The efficiency of hole cleaning is greatly improved by increasing the rotational speed of drillpipe, flow rate of drilling fluid, remover eccentricity, and 6 rpm Fann dial reading for drilling fluid. While higher rate of penetration and large wellbore size result in worse hole cleaning. These findings can serve as an important guide for the structure optimization design of cuttings bed remover and installation spacing of removers.

1. Introduction

In extended-reach and horizontal well drilling processes, drilling cuttings continuously deposit to the bottom of the wellbore and form cuttings bed by the force of gravity (Busch and Johansen, 2020; Ramsey, 2019). Cuttings bed may lead to complex downhole problems, such as high torque and drag, noticeable reduction of ROP, and loss of well control, which poses severe threats to the operation safety and drilling efficiency (Pang et al., 2019; Chen et al., 2016; Hovda, 2019). Although many measures have been taken to clean wellbore, accidents still occur sometimes. For example, in the extended-reach well of Long 40-1 of Sichuan Oilfield, poor hole cleaning caused multiple drill pipes sticking (Wang et al., 1995). In some areas, events related to differentially stuck pipe can be responsible for nearly 40% of the total well cost (Siruvuri et al., 2006). Therefore, further study on hole cleaning is the key to reducing such down-hole accidents.

According to previous research, there are several effective measures for cuttings bed cleaning (Lockett et al., 1993; Li and Walker, 2001; Ofei et al., 2015; Huque et al., 2020), including increasing the velocity of drilling fluid and drillpipe rotational speed, improving drilling fluid performances, etc. Wang et al. (1995) explored drilling cuttings transport in a horizontal well, noting that pipe rotation significantly reduces bed height at low flow rates but has no substantial effect at high flow rates. Duan et al. (2008) studied small cuttings transport in extended-reach drilling, examining the impacts of cuttings size, drill pipe rotation, fluid rheology, flow rate, and hole inclination both experimentally and

* Corresponding author.
** Corresponding author.
E-mail addresses: huangwenjun1986@126.com (W.-J. Huang), gaodeli_team@126.com (D.-L. Gao).

https://doi.org/10.1016/j.petsci.2024.03.006

theoretically. In a Computational Fluid Dynamics (CFD) study, Bilgesu et al. (2007) simulated solid-liquid two-phase flows in wellbore annuli, revealing drill pipe rotation can improve cutting transport more for smaller sized particles. Sun et al. (2014) used CFD to simulate the effects of drill pipe rotation on cuttings transport in the complex structure well with an Euler multiphase model. They concluded that pipe rotation significantly impacts annular cuttings distribution in inclined sections. Ford et al. (1990) conducted experiments related to the flow of Power Law Fluids in annuli, finding improved hole cleaning with increased viscosity. Rishi et al. (2000) investigated cuttings bed height over time with variable flow rates (200–400 gpm) and four drilling fluid compositions, revealing a lower cuttings bed height with an increased n/k ratio. Almost all of the studies revealed that non-Newtonian fluid plays a vital role in cuttings transport. Despite these insights, cuttings bed generation is usually inevitable in larger-diameter wellbores, such as 17½" and 12¼" sections, even under significant drilling fluid flow rates and high drill string rotational speeds (rpm). In such case, cuttings bed removers can destroy the amassed cuttings bed, lift the cuttings to the high-velocity flow zone in the upper annulus section, and thus improve the efficiency of hole cleaning (Ramadan et al., 2011).

In recent years, the remarkable progress in computer performance has facilitated the utilization of computational fluid dynamics (CFD) numerical simulation methods for studying the removal of cuttings bed. Cao et al. (2019) proposed a design of cuttings bed remover with spiral grooves, established a three-dimensional model of the cuttings bed remover with different structural parameters, and analyzed its capability to carry the cuttings with CFD simulation. Puymbroeck and his collaborators (Van Puymbroeck and El Bachiri, 2013; Van Puymbroeck and Williams, 2013) invented a cuttings remover with double spiral grooves (hydroclean TM). The field application showed that this tool has an excellent effect on cuttings bed removal. Boulet et al. (2000) developed a new tool with two grooves of hydraulic cleaning areas and hydraulic bearing areas and studied the hydraulic cleaning effect of the grooves by numerical simulation. The researchers have carried out extensive studies on the hole cleaning performance of cuttings bed removers with various structural parameters. However, most studies utilize a Newtonian fluid as the cuttings-carrying fluid and consider small hole sizes, without simulating the effects of actual fluid properties, hole conditions, and other parameters on cuttings transport near the cuttings bed remover.

There are several theoretical and empirical methods for evaluating hole cleaning effect (Saasen, 1998; Awad et al., 2022; Miao et al., 2023; Brett et al., 1989). The cleanliness of the hole can be evaluated by measuring the thickness of the cuttings bed. However, due to the redistribution and accumulation of cuttings, accurately measuring the actual thickness becomes challenging. The cuttings transport ratio relies on the concentration of cuttings in the returned drilling fluid to indicate hole cleanliness. However, its accuracy may be influenced by well depth and diameter. The accumulation of cuttings can affect the equivalent circulating density (ECD) by decreasing the open flow area and increasing the average density of the drilling fluid. The hole cleaning effect can be detected by monitoring changes in the ECD. However, factors influencing the variation of ECD include not only the cuttings bed but also the annular flow area, rate of penetration, and wellbore structure. The friction coefficient can reflect the hole cleaning effect, but various factors, such as wellbore structure and wall stability, introduce uncertainties. These methods for hole cleaning evaluation have their respective limitations, rendering them unsuitable for a rapid and quantitative assessment for the cuttings bed remover's hole cleaning capability.

The number and spacing of cuttings bed removers are also closely related to the hole cleaning effect. As the number of cuttings bed removers increases, the hole cleaning effect improves. However, too many cuttings bed removers may cause excessive Equivalent Circulating Density (ECD) and torque, posing serious threats to drilling safety. Meanwhile, installing removers with too large or small spacing leads to inadequate hole cleaning. Therefore, there are optimal values for cuttings bed remover's number and installation spacing. However, there is still a lack of a design method to use cuttings bed removers efficiently.

The purpose of this study is to develop a rapid and quantitative evaluation index for assessing the cleaning effectiveness of a cuttings bed remover. Based on fluid mechanics and the wellbore cleaning mechanisms of cuttings bed removers, a new cuttings bed remover with streamline blades was designed. Subsequently, based on this evaluation index, the impacts of drilling parameters on the tool's performance were studied. Next, by calculating the average cuttings concentration in the annulus, the reasonable design method for the installation spacing of cuttings bed removers was established. Finally, these studies were applied to an extended-reach well in the South China Sea, and the results showed an improvement in wellbore cleaning effectiveness.

2. Model and methodology

The overall processes has been summarized in Fig. 1. Further specifics are presented in the following sections.

2.1. A new design of cuttings bed remover

2.1.1. Wellbore clean mechanisms of cuttings bed removers

In the drilling process, the drill bit breaks the rock into small cuttings, and the cuttings are transported to the surface through the wellbore annulus by circulating drilling fluid. However, since the density of drilling cuttings is higher than that of drilling fluid, it gradually settles down at the lower side of the annular section due to gravity. If the generated cuttings are not adequately removed from the hole section, it will trigger the formation of the cuttings bed on the wellbore bottom. According to the transportation states of cuttings, the whole wellbore annulus can be mainly divided into three layers, including a fixed layer at the bottom, a diffusion layer above it, and a suspension layer at the top (Nguyen and Rahman, 1996; Cho et al., 2002; Wang and Long, 2010). The cuttings in the fixed layer lie still on the lower side, and it is difficult for the cuttings to jump into the upper high-velocity flow zone, which is the main reason for the uncleanness of the wellbore.

Spiral grooves are usually processed on the body of cuttings bed removers, or blade structures of different geometries are arranged on removers. Both body ends are connected with the drillpipe by the internal and external thread joints. The mechanisms of cuttings bed removers assisting in hole cleaning can be divided into two aspects: mechanical action and hydraulic action (Yan et al., 2014; Van Puymbroeck, 2013).

For the mechanical action, the blade's outer edge of the remover cuts into the cuttings bed and scrapes the mud cake or cuttings on the well wall while rotating. Then, the motion pattern of cuttings changes from the compacted state to the free state. Meanwhile, a considerable number of cuttings will be rolled up by the blade to the upper annulus and then discharged from the upper annulus by the high axial velocity fluid field, as described in Fig. 2.

For the hydraulic action, the swirl flow around the wellbore axis is generated when the drilling fluid flows through the grooves and blades of the remover, as depicted in Fig. 3. Under swirl flow, the surface cuttings gradually separate from the cuttings bed and move to the suspension layer through the diffusion layer. At the same

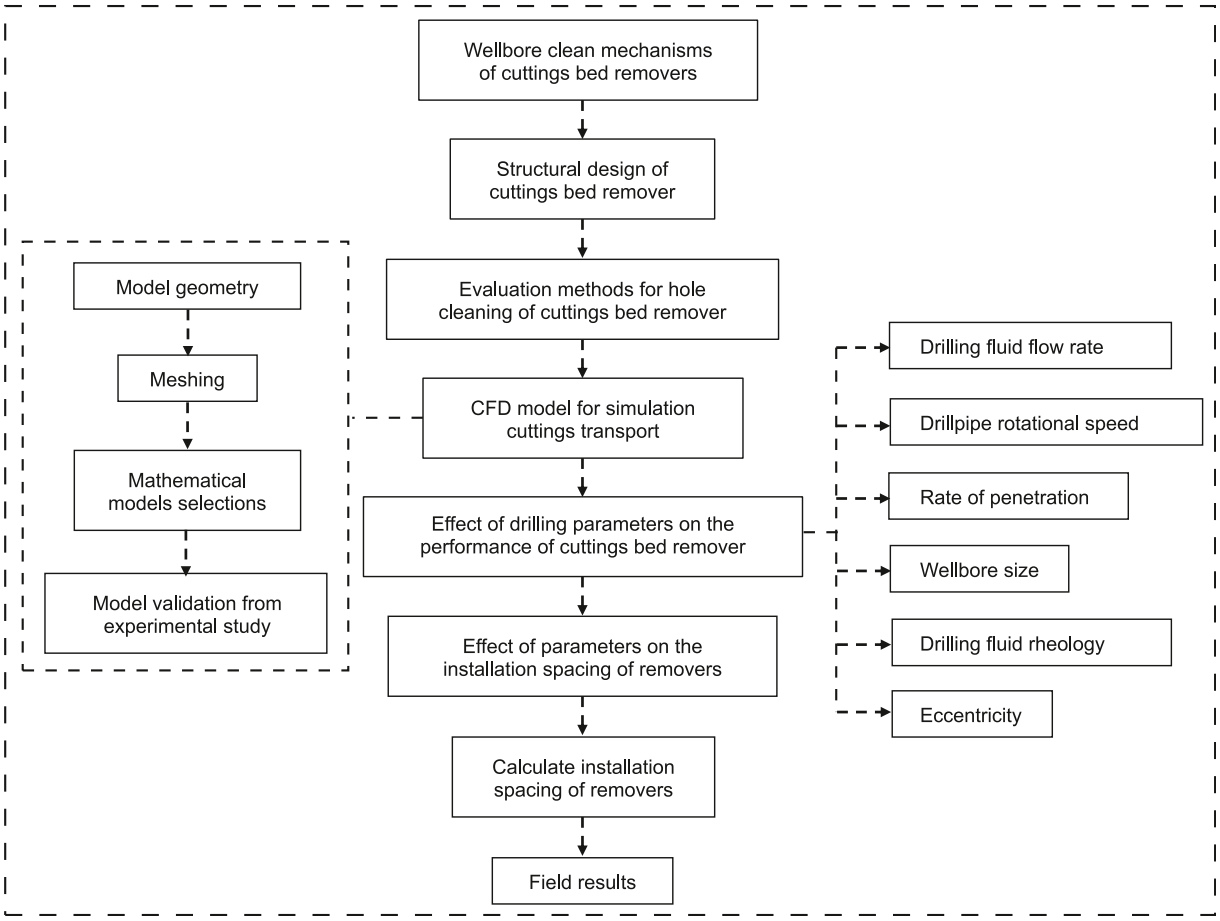

Fig. 1. Overall flow chart illustrating the study processes.

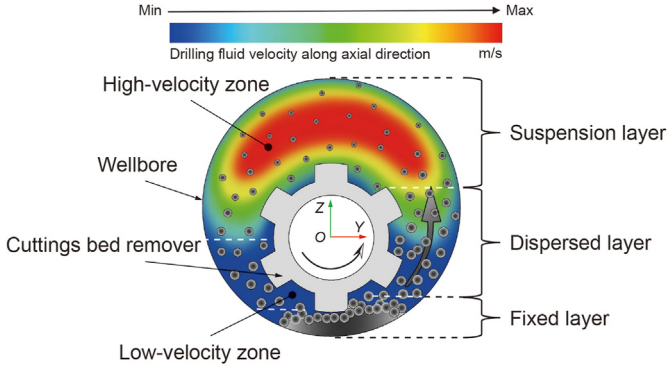

Fig. 2. Cuttings transport patterns with the remover rotation in the horizontal wellbore.

time, the rotation of the remover disturbs the annulus flow field and tremendously improves the turbulence intensity of the fluid field. As a result, the deposition of cuttings at the bottom of the annulus is impeded, and the thickness of the cuttings bed is significantly reduced.

2.1.2. Geometry model of streamlined blade cuttings bed remover

In the last few decades, many researchers have designed different types of cuttings bed removers to improve the hole cleaning efficiency. Unreasonable blade shape may lead to poor cuttings migration and reduce the penetration rate.

To improve the effectiveness of cuttings bed removers, the authors designed a new cuttings bed remover with streamline blades, which has a better hole cleaning effect than other types of removers through quantitative evaluation. Streamlined blades offer serval following advantages over traditional blades: As the streamlined blades rotate, numerous vortices generate near the base of the streamlined blades, causing local turbulent flow in the annular space. This turbulent effect enhances the mixing of cuttings and drilling fluid, preventing the accumulation of cuttings on the remover surface. Consequently, it inhibits the formation of mud packing on the remover's exterior. In addition, the concave arc surface of the streamlined blades facilitates the transport of a greater quantity of cuttings to the upper annulus compared to traditional blades. This enhancement contributes to the overall effectiveness of the cuttings bed removers.

The remover is sketched in Fig. 4, which consists of joint sections at both ends of the tool and the middle working section. Blade structures or grooves of various shapes are uniformly distributed around the working section. There are two necks as smooth transition sections between the joint sections and the working section. The transition section contributes to establish a smooth connection between the working and joint sections. This element is commonly set up with a diameter that gradually decreases, helping to regulate the flow of drilling fluid and facilitating cuttings entry into the joint section. The design of the transition section plays a crucial role in preventing blockages and optimizing the efficiency of the remover. Utilizing the threads on the joint section, the cuttings bed remover is integrated between the drill pipes.

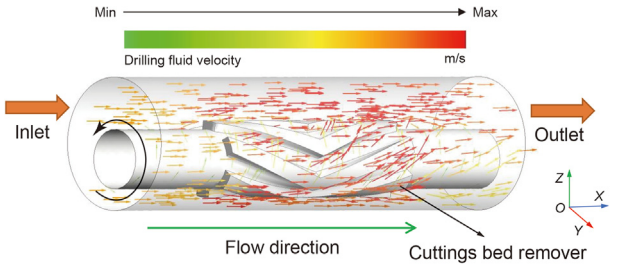

Fig. 3. The 3D streamline of the annulus fluid.

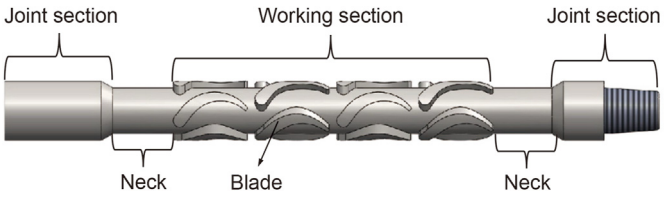

Fig. 4. Schematic diagram of the streamline blade cuttings bed remover.

Fig. 5 shows the schematic diagram of the streamline blade. The main structural parameters of the blades include: r_1 and r_2 are the semicircle radii of the front and rear ends of the blade, respectively; R_1 and R_2 are the inner and outer arc radii, respectively; a is the axial height of the blade; c is the chord length of the blade; h is the height of the blade. The flow parameters mainly include liquid inflow angle β_1 and liquid outflow angle β_2.

2.2. Evaluation methods

In previous studies, the hole cleaning effect was mainly evaluated from the aspects of the changes in physical quantities, including concentration distribution of drilling cuttings in the wellbore, average flow velocity in the annulus, and so on (Heydari et al., 2017; Sun et al., 2017; Yan et al., 2020). Until now, there has not been a quantitative index to measure the hole cleaning effect directly. In this paper, two evaluation indexes are proposed to evaluate the effects on the performance of cuttings bed remover, including the transverse velocity of mixed fluid consisting of drilling fluid and cuttings and the cleanliness factor. The transverse velocity refers to the component of fluid velocity along a direction perpendicular to the axis within the cross-section of the annulus. It

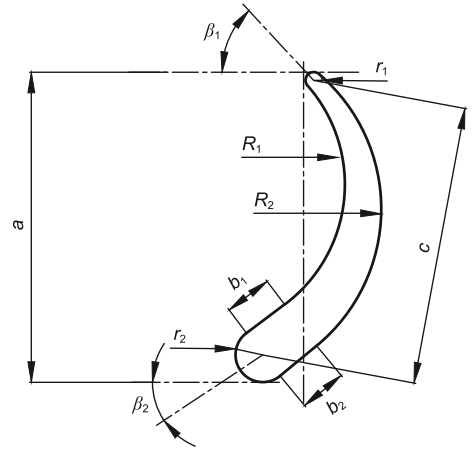

Fig. 5. Schematic diagram of the streamline blade.

indicates the intensity of the turbulence effect of the fluid and provides a transverse impact force of drilling fluid on the cuttings bed. For this reason, higher transverse velocity helps the cuttings easily jump and diffuse to the high-velocity zone in the annulus, and thus the performance of the tool is better.

The cleanliness factor is calculated by:

$$Q = \frac{1}{t_2 - t_1} \cdot \int_{t_1}^{t_2} \frac{\iint \frac{1}{c} v_2 \mathrm{d}A}{\iint v_1 \mathrm{d}A} \mathrm{d}t \tag{1}$$

where Q is the cleanliness factor; A is the cross-section area of the annulus; c is the volume fraction of drilling cuttings; v_1 is the axial component of velocity after mixing fluid and cuttings; v_2 is the component of the velocity perpendicular to the axis after mixing the fluid and drilling cuttings in the annulus, i.e., the transverse component; t_1 represents the time when the simulation process tends to steady-state, and t_2 represents the end time of the numerical simulation.

The integrand function of Eq. (1) represents the ratio of the transverse component of fluid and cuttings flow to the axial component. The numerator of the integrand function of Eq. (1) is the integral of the product of the reciprocal of transverse velocity and cuttings volume fraction on Section A, and the denominator is integral in the axial direction. According to the cleanliness factor, an enhanced stirring effect of the remover results in higher cleanliness. Furthermore, lower volume fractions of cuttings in the wellbore correspond to increased cleanliness. These patterns are reasonable, so cleanliness can be an essential index for evaluating the stirring effect. To comprehensively evaluate the cleaning effect in the remover, the above two evaluation indexes are both adopted.

2.3. CFD model and parameter settings

In this paper, the Eulerian-Eulerian (EE) multiphase model was utilized to simulate the transient solid-liquid two-phase flow in the annulus. The EE multiphase model treats the particles as a continuous medium like the fluid phase, which is more efficient than the Eulerian-Lagrangian model and is widely applied in engineering. The dynamic mesh capability of ANSYS Fluent 18.0 is exploited to account for the uniform rotational motion of the remover. The exchange of momentum and energy between the solid and liquid phases was mathematically represented as additional source terms in the conservation equation. The interaction was achieved through the interphase forces. For simplicity, the following assumptions were considered in developing the CFD model.

1. Drilling fluids were treated as incompressible non-Newtonian fluids, and the rheology meets the Herschel-Bulkley rheological model.
2. The impact of the uneven surface of the cuttings was disregarded. Consequently, the cuttings were assumed mono-sized spherical geometries with a uniform density. Cuttings are assumed to remain intact and not broken or coalesce during migration.
3. The heat transfer and mass exchange in solid and liquid phases were not considered.

Fig. 6 outlines the numerical simulation procedure used to obtain the results.

2.3.1. Governing equations

The dynamic mesh model is suitable for simulating flows in

which the shape of the domain changes with time due to motion on the domain boundaries. For dynamic meshes, the integral form of the conservation equation for a general scalar, φ, on an arbitrary control volume, V, with a moving boundary, can be formulated as (Busch and Johansen, 2020):

$$\frac{\mathrm{d}}{\mathrm{d}t}\int_V \rho\varphi \mathrm{d}V + \int_{\partial V} \rho\varphi\left(\vec{u}-\vec{u}_g\right)\cdot \mathrm{d}\vec{A} = \int_{\partial V} \Gamma\nabla\varphi\cdot \mathrm{d}\vec{A} + \int_V S_\varphi \mathrm{d}V \quad (2)$$

where ρ is the fluid density; $\vec{u}$ is the velocity vector of the flow; $\vec{u}_g$ is the mesh velocity of the moving mesh; Γ is the diffusion coefficient; S_φ is the source term of φ; $\vec{A}$ is the areal vector of the control volume; ∂V is used to represent the boundary of the control volume, V.

The continuity equation and momentum equation are established in the Eulerian coordinate system, respectively (Van Wachem and Almstedt, 2003).

The continuity equations for drilling fluid and cuttings can be expressed as follows:

$$\frac{\partial}{\partial t}(\alpha_\mathrm{l}\rho_\mathrm{l}) + \nabla\cdot\left(\alpha_\mathrm{l}\rho_\mathrm{l}\vec{u}_\mathrm{l}\right) = 0 \quad (3)$$

$$\frac{\partial}{\partial t}(\alpha_\mathrm{s}\rho_\mathrm{s}) + \nabla\cdot\left(\alpha_\mathrm{s}\rho_\mathrm{s}\vec{u}_\mathrm{s}\right) = 0 \quad (4)$$

where l and s represent the drilling fluid and cuttings, respectively. α, $\vec{u}$, and ρ is the volume fraction, velocity vector, and density, respectively

The momentum equation for drilling fluid and cuttings is represented by the following equations (Amanna and Movaghar, 2016):

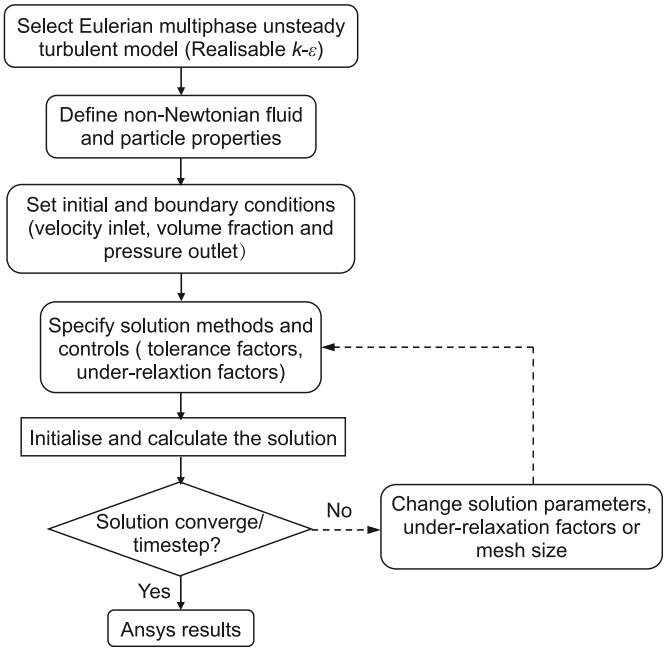

Fig. 6. Simulation procedure for the EE multiphase model.

$$\frac{\partial}{\partial t}\left(\alpha_\mathrm{l}\rho_\mathrm{l}\vec{u}_\mathrm{l}\right) + \nabla\cdot\left(\alpha_\mathrm{l}\rho_\mathrm{l}\vec{u}_\mathrm{l}\vec{u}_\mathrm{l}\right) = -\alpha_\mathrm{l}\nabla p + \alpha_\mathrm{l}\nabla\cdot\bar{\bar{\tau}}_\mathrm{l} + \alpha_\mathrm{l}\rho_\mathrm{l}\vec{g} - \beta\left(\vec{u}_\mathrm{l}-\vec{u}_\mathrm{s}\right) + F_{\mathrm{lift,l}} + F_{\mathrm{vm,l}} \quad (5)$$

$$\frac{\partial}{\partial t}\left(\alpha_\mathrm{s}\rho_\mathrm{s}\vec{u}_\mathrm{s}\right) + \nabla\cdot\left(\alpha_\mathrm{s}\rho_\mathrm{s}\vec{u}_\mathrm{s}\vec{u}_\mathrm{s}\right) = -\alpha_\mathrm{s}\nabla p - \nabla p_\mathrm{s} + \alpha_\mathrm{s}\nabla\cdot\bar{\bar{\tau}}_\mathrm{s} + \alpha_\mathrm{s}\rho_\mathrm{s}\vec{g} + \beta\left(\vec{u}_\mathrm{l}-\vec{u}_\mathrm{s}\right) + F_{\mathrm{lift,s}} + F_{\mathrm{vm,s}} \quad (6)$$

where $\vec{g}$ is the acceleration of gravity; $\bar{\bar{\tau}}$ is the stress tensor; p is the pressure shared by all the phases; p_s is the solid pressure; β is the momentum exchange coefficient between the fluid and solid phases. F_{lift}, F_{vm} are the lift force and the virtual mass force, respectively.

When it comes to simulating flows that exhibit separation, involve boundary layers with high-pressure gradients, or contain complex flow structures, the realizable k-ε turbulence model is often considered to be more accurate than other k-ε models (Araoye et al., 2017). The transport equations for turbulence kinetic energy (TKE) and its dissipation rate in the realizable k-ε model can be expressed as follows (Yan et al., 2019):

$$\frac{\partial(\rho_\mathrm{l}k)}{\partial \mathrm{t}} + \frac{\partial\left(\rho_\mathrm{l}k\vec{u}_\mathrm{j}\right)}{\partial x_\mathrm{j}} = \frac{\partial}{\partial x_\mathrm{j}}\left[\left(\mu+\frac{\mu_\mathrm{t}}{\sigma_k}\right)\frac{\partial k}{\partial x_\mathrm{j}}\right] + G_\mathrm{k} - \rho_\mathrm{l}\varepsilon \quad (7)$$

$$\frac{\partial(\rho_\mathrm{l}\varepsilon)}{\partial \mathrm{t}} + \frac{\partial\left(\rho_\mathrm{l}\varepsilon\vec{u}_\mathrm{j}\right)}{\partial x_\mathrm{j}} = \frac{\partial}{\partial x_\mathrm{j}}\left[\left(\mu+\frac{\mu_\mathrm{t}}{\sigma_\varepsilon}\right)\frac{\partial \varepsilon}{\partial x_\mathrm{j}}\right] + \rho_\mathrm{l}C_1S\varepsilon - \rho_\mathrm{l}C_2\frac{\varepsilon^2}{k+\sqrt{\frac{\mu}{\rho_\mathrm{l}}\varepsilon}} \quad (8)$$

where μ is the dynamic viscosity; μ_t is the turbulent viscosity; k is the turbulence kinetic energy; ε is the dissipation rate; σ_k and σ_ε are the turbulent Prandtl numbers of the k equation and ε equation, respectively. C_1 and C_2 are the two constants; G_k represents the generation of turbulence kinetic energy due to mean velocity gradients; S is the modulus of the mean rate of strain tensor.

The constitutive equation of non-Newton fluid with the Herschel-Bulkley rheological model can be expressed mathematically as (Rooki et al., 2015):

$$\tau = \tau_0 + K\gamma^n \quad (9)$$

where τ is the shear stress; τ_0 is the yield stress; K is the consistency coefficient; γ is the shear rate; n is the flow index.

2.3.2. Boundary conditions and initial conditions

In the two-phase flow system simulation, velocity-inlet and pressure-outlet boundary conditions were used at the inlet and outlet, respectively. The outlet pressure was set to the ambient atmospheric pressure. The wellbore wall was assumed to be static, without gaps and cracks, while the outer wall of the remover was treated as a moving boundary. A no-slip velocity boundary condition was applied to the walls. The system consisted of a drilling fluid and uniformly dispersed cuttings that entered the annulus through the inlet and exited through the outlet. The main geometrical parameters and operating conditions summarized in the simulation are listed in Table 1.

The governing equations were discretized using the finite volume method on each cell along the annulus, with pressure discretization being implemented according to the Semi-Implicit

Method for Pressure-Linked Equations (SIMPLE) scheme. The momentum equations were solved using second-order implicit time integration, and the Quadratic Upstream Interpolation for Convective Kinematics (QUICK) method was selected for volume fraction interpolation. The commercial software ANSYS Fluent 18.0 was used to perform the CFD simulation for the above-described strategy. The time step for convergence was selected as 1×10^{-4} s.

2.3.3. Computational mesh and mesh independence study

Fig. 7 illustrates the geometry of the remover, of which the geometrical parameters are listed in Table 2. When the wellbore size is 215.9 mm, the cuttings bed removers employs blades with a height of 10.15 mm.

The swirl flow field was divided by unstructured tetrahedral mesh. Compared with the structured grid, it can reduce skewness and obtain better mesh quality for complex computing domains. Considering that the flow situation near the blades and the grooves is considerably complex, the meshes near the working section were refined to reduce the calculation error. When the remover rotates at a uniform speed, the surrounding meshes are continuously updated by dynamic smoothing and remeshing.

As shown in Fig. 8, the movement of the two-phase flow can be decomposed into the axial direction (along the wellbore) and transverse velocity direction (perpendicular to the wellbore). The blade segment is the core part of the cuttings bed remover, which has the most significant effect on hole cleaning, and the effects of other parts are relatively minor and can be ignored. The relevant simulation parameters are shown in Table 1, and the distributions of cleanliness for the different ratios of simulated annulus length to hydraulic diameter are shown in Fig. 9. The results indicate that the results are nearly irrelevant to the ratio of length to hydraulic diameter when the ratio is not smaller than 26. To guarantee computational efficiency and accuracy, the simulated length of the annulus was set to 2 m (the ratio of length to hydraulic diameter is about 26).

Mesh independence study was conducted by varying mesh size and then computing the mean transverse velocity of drill fluid in the outlet plane. The boundary conditions and initial conditions are shown in Table 1. Fig. 10 demonstrates that when the mesh size reaches about 4×10^5, further increasing mesh size has a negligibly small effect on the result. Therefore, to improve the calculation speed meanwhile ensure accuracy, the mesh size was optimized to about 4×10^5. The computational domain mesh is shown in Fig. 11.

Table 1
Geometrical parameters and operating conditions summarized in the numerical simulation.

Symbol	Parameters	Simulation values
Geometry		
D_h	Hole diameter, mm	215.9, 311.15, 444.5
D_p	Drillpipe diameter, mm	139.7
L	Computational length, m	2
Particle properties (spherical)		
D_s	Cuttings diameter, mm	1
ρ_s	Cuttings density, kg/m^3	2500
Drilling fluid properties		
ρ_1	Fluid density, kg/m^3	1200
τ_0	Yield stress, Pa	0, 5, 10, 15
K	Consistency index, (Pa·s^n)	0.05, 0.1, 0.2
n	Flow behaviour index	0.4, 0.5, 0.6, 0.8, 1
Drilling variables		
ROP	Rate of penetration, m/h	20, 30, 40, 50
v	Annulus flow rate, L/s	25, 35, 40, 45, 50, 60
ω_d	Drillpipe rotation, rpm	40, 60, 80, 90, 120, 150
γ	Wellbore inclination, °	90
E	Eccentric distance, mm	0, 10, 20, 30, 40
e	Eccentricity ($e = E/(D_h/2\text{-}D_p/2)$	0, 0.125, 0.25, 0.375, 0.5

3. Results and discussion

3.1. CFD model validation

To validate the accuracy of CFD model, the simulation results were compared with the experiments which were performed in the "Drilling Laboratory of the Tehran Polytechnic University" in Petroleum Engineering Department (Amanna and Movaghar, 2016).

Four tests have been taken in laboratory by considering 60 angle, cutting size of 5 mm diameter, pipe rotation of 60 rpm and different flow rates and corresponding CFD simulations have then been performed. The experiments used water as a carrier for transporting cuttings, with sand injected into the annulus with fluid from the inlet simultaneously. The inlet velocity of sand was the same as that of the fluid, while the constant and input parameters were set to the same values as in the experiment described in Ref. (Amanna and Movaghar, 2016). The main simulation parameters are listed in Table 3.

Comparing the curves referring to simulation and experimental results regarding cuttings in annular space to total cuttings injected at different drilling fluid flow rates in Fig. 12, a mean relative percentage error of 3.6% is observed. The good agreement between the numerical simulation results and the experimental data demonstrates the reliability of the CFD simulation model used in the study.

3.2. Analysis of fluid field characteristics of remover

Specific vortexes around blades are created under the effect of remover rotation. The size and number of vortexes play a crucial role in determining cleaning efficiency of the cuttings bed removal (Yan et al., 2019; Zhou et al., 2018).

Based on the relevant parameters in Table 1, the distribution features of vortexes are obtained by employing CFD numerical simulations on cuttings bed removers with streamline blades. Four cross-sections were selected to comprehensively monitor the fluid flow characteristic, in which plane-1 and plane-2 are located in the middle of the blades, and plane-3 and plane-4 are located behind the blades. The axial positions of four planes are 0.9, 1.15, 1.6 and 1.8 m. The distributions of streamlines on four cross-sections are shown in Fig. 13.

It can be found from Fig. 13(a) and (b) that the streamlines in plane-1 and plane-2 are more disordered, some vortexes have formed near the blades and the grooves, as shown in areas 1 and 2. These vortexes result in easier suction of drilling cuttings into the grooves. Subsequently, under centrifugal force from fluid, cuttings are thrown to the high side of the annulus, then discharged with the fluid flow. As shown in areas 1, 2, and 3, the vortexes in plane-3 are relatively smaller than in plane-1 and plane-2, indicating that the size of vortexes gradually decreases due to the viscous resistance. Moreover, as the vortexes gradually disappear, the fluid flow directions tend to be consistent, as shown in Fig. 13(d).

3.3. Comparison of four removers

Common removers have several kinds of blades, including

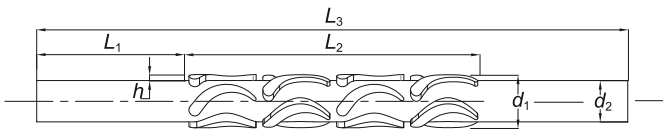

Fig. 7. Geometry of the streamline blade cuttings bed remover.

Table 2
Geometrical parameters of the streamline blade cuttings bed remover.

Symbol	Parameters	Simulation values
d_1	Outer diameter, mm	160/180
d_2	Neck diameter, mm	139.7
L_1	Length of neck, m	0.5
L_2	Length of working section, m	1
L_3	Computational length, m	2
h	Blade height, mm	10.15/20.15
r_1	Semicircle radii of the front, mm	6
r_2	Semicircle radii of the ends, mm	20
R_1	Inner arc radii, mm	110
R_2	Outer arc radii, mm	130
a	Axial height of blade, mm	230
b	Chord length of blade, mm	35
β_1	Liquid inflow angle, °	50
β_2	Liquid outflow angle, °	35

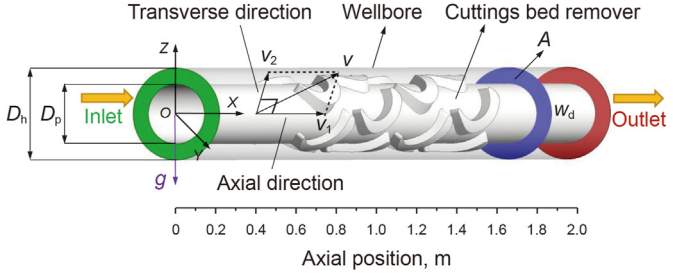

Fig. 8. Schematic diagram of the streamline blade cuttings bed remover.

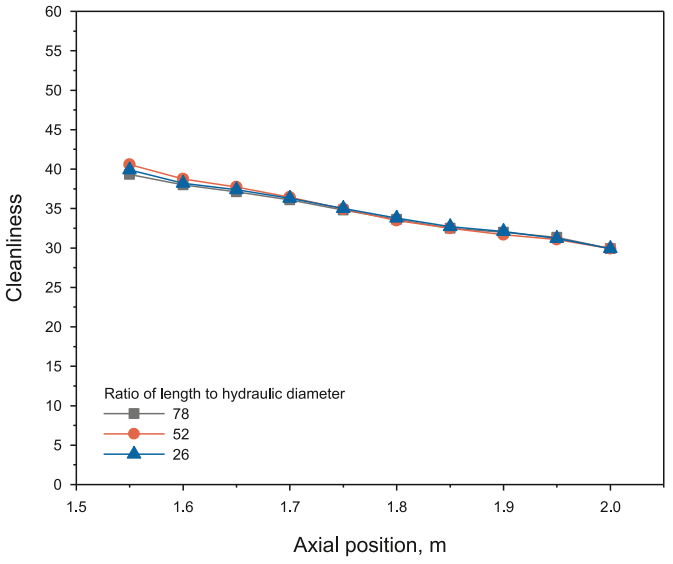

Fig. 9. Variation of cleanliness at different ratios of length to hydraulic at: ROP = 40 m/h, ω_d = 60 rpm, v = 35 L/s, D_h = 215.9 mm, e = 0, τ_0 = 5 Pa, K = 0.1 Pa·s^n, n = 0.5.

straight blade, spiral blade, "V" blade, and cross combinations of different kinds of blades.

Fig. 14 illustrates the geometry of three kinds of cuttings bed removers. The turning angle θ of the "V" blade is 170°, the helix angle α of the positive spiral blade is 5°, and all blades' width δ is 40 mm. The common removers has several blades, and CFD simulation is carried out under the same simulation conditions. According to the evaluation indexes proposed in this paper, the four kinds of removers are evaluated, and the results are shown in Figs. 15 and 16.

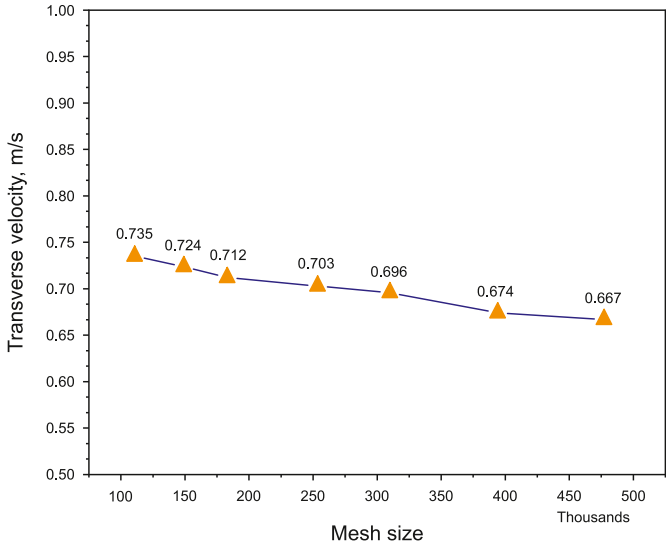

Fig. 10. Mesh independence test at: ROP = 40 m/h, ω_d = 60 rpm, v = 35 L/s, D_h = 215.9 mm, e = 0, τ_0 = 5 Pa, K = 0.1 Pa·s^n, n = 0.5.

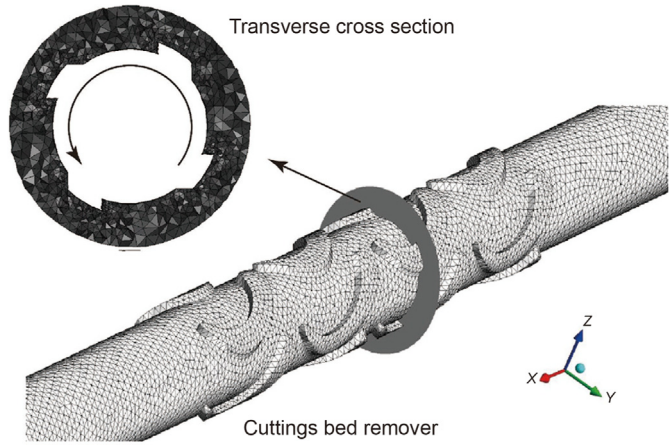

Fig. 11. Computational domain and mesh used in the simulations.

Table 3
Data used for validation of the numerical solution against the experimental data.

Symbol	Parameters	Simulation values
Geometry		
D_h	Hole diameter, mm	57.15
D_p	Drillpipe diameter, mm	104.78
L	Computational length, m	4
Particle properties (spherical)		
D_s	Diameter, mm	5
ρ_s	Density, kg/m^3	2700
Drilling fluid properties		
	Fluid type	water
μ_1	Density, kg/m^3	998.2
Drilling variables		
v	Annulus flow rate, gpm	40–90
ω_d	Drillpipe rotation, rpm	0
	Flow regime	Turbulent flow
γ	Wellbore inclination, °	60
-	Inlet cutting volume fraction	0.06
e	Eccentricity	0

Fig. 15(a) shows that all the four removers have an excellent performance. However, the cleaning effect of streamline blade

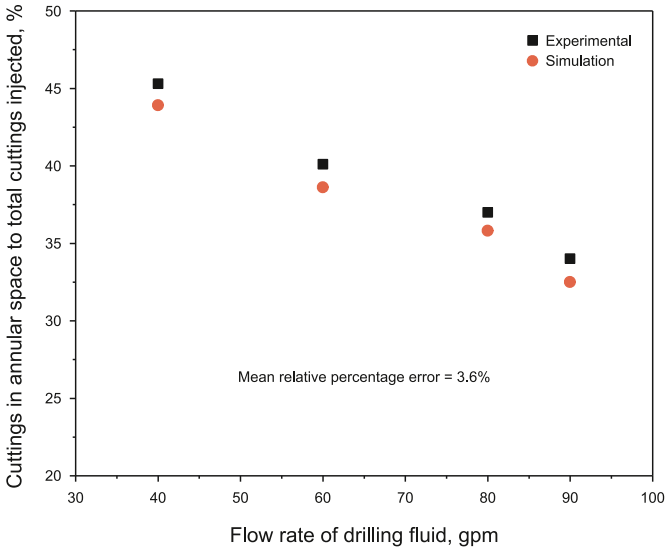

Fig. 12. Comparison of simulations with experiments.

cuttings bed remover is better than that of "V" blade cuttings bed remover, followed by straight blade remover. The effect of positive spiral remover is the weakest.

Fig. 15(b) shows that the transverse velocity near four tools increases first and then decreases, the transverse velocity near streamline blades at the highest level compared with other removers. The transverse velocity near "V" blade remover presents a similar trend with spiral blade remover at the axial position of 0.5–1 m. It rapidly rises to a peak value of 0.54 m/s at the axial position of 1.45 m. The probable reason is that the transition of the spiral direction of "V" blade changes the flow direction of drilling fluid, thereby enhancing the turbulence intensity of the surrounding fluid. The above results indicate that the spiral direction of blade has a positive influence on performance of remover.

As vividly presented in Fig. 16, the transverse velocity near streamline remover is higher than others, which will effectively prevent the formation of the cuttings bed.

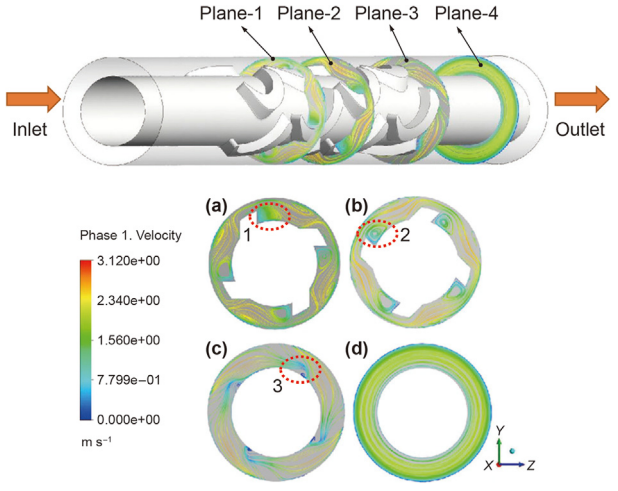

Fig. 13. The streamline in the section plane at: ROP = 40 m/h, ω_d = 60 rpm, v = 35 L/s, D_h = 215.9 mm, e = 0, τ_0 = 5 Pa, K = 0.1 Pa·s^n, n = 0.5. (**a**) Plane-1. (**b**) Plane-2. (**c**) Plane-3. (**d**) Plane-4.

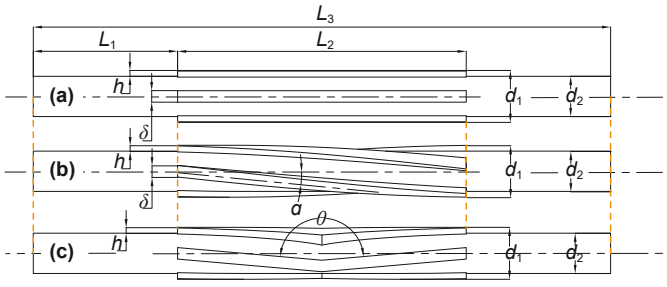

Fig. 14. Geometry of three kinds of cuttings bed removers. (**a**) Straight blade cuttings bed remover. (**b**) Positive spiral cuttings bed remover. (**c**) "V" blade cuttings bed remover.

3.4. Effect of drilling parameters on the performance of cuttings bed remover

In this section, the impacts of several drilling parameters on the performances of removers are discussed through some indicative factors of drilling fluid flow rate, drillpipe rotational speed, rate of penetration (ROP), wellbore size, drilling fluid rheology, and eccentricity.

3.4.1. Effect of drilling fluid flow rate

Fig. 17(a) and (b) show the influence of the drilling fluid flow rate on the wellbore cleanliness and transverse velocity. The axial position in the figure means the distance away from the annulus inlet along the wellbore axis.

Fig. 17(a) shows that increasing the drilling fluid flow rate is conducive to enhancing the cleanliness of the remover. The cleanliness goes up rapidly from 54.5 to 66.5 as the flow rate increases from 25 to 45 L/s. Simultaneously, the cleanliness of the wellbore decreases sharply along the flow direction due to the friction loss of the pipe wall and the viscous shear effect of the fluid.

The transverse velocity of the fluid dramatically increases as the flow rate increases from 25 to 45 L/s in the annulus, as shown in Fig. 17(b). It is evident from the data that the transverse velocity exhibits erratic fluctuations around the working section. The intricate design of the remover, coupled with variations in the drilling conditions, leads to erratic fluctuations on the transverse velocity. At a higher flow rate, the cutting particles are more evenly distributed and easier to lift from the bottom bed layer to the upper high-velocity flow. Unfortunately, the drilling fluid flow rate is limited by the drill pump, and too high flow rates can result in severe wellbore erosion. Consequently, the flow rate should be controlled in a proper range to ensure drilling safety and hole cleaning.

3.4.2. Effect of drillpipe rotational speed

Fig. 18(a) and (b) show the influence of the drillpipe rotational speed on the wellbore cleanliness and transverse velocity. According to Fig. 18(a), the initial wellbore cleanliness is positively correlated with rotational speed. The results indicate that the improvement in performance due to an increase in rotational speed is less significant at high speeds compared to low speeds. Furthermore, the improvement becomes negligible beyond a rotation of 120 rpm, making further rotation unnecessary.

Fig. 18(b) shows that the transverse velocity near the remover increases with increasing rotational speed. Under higher transverse velocity, the cuttings accumulation tendency will be significantly alleviated. Nevertheless, higher drillpipe rotational speed requires more power for mud pumping.

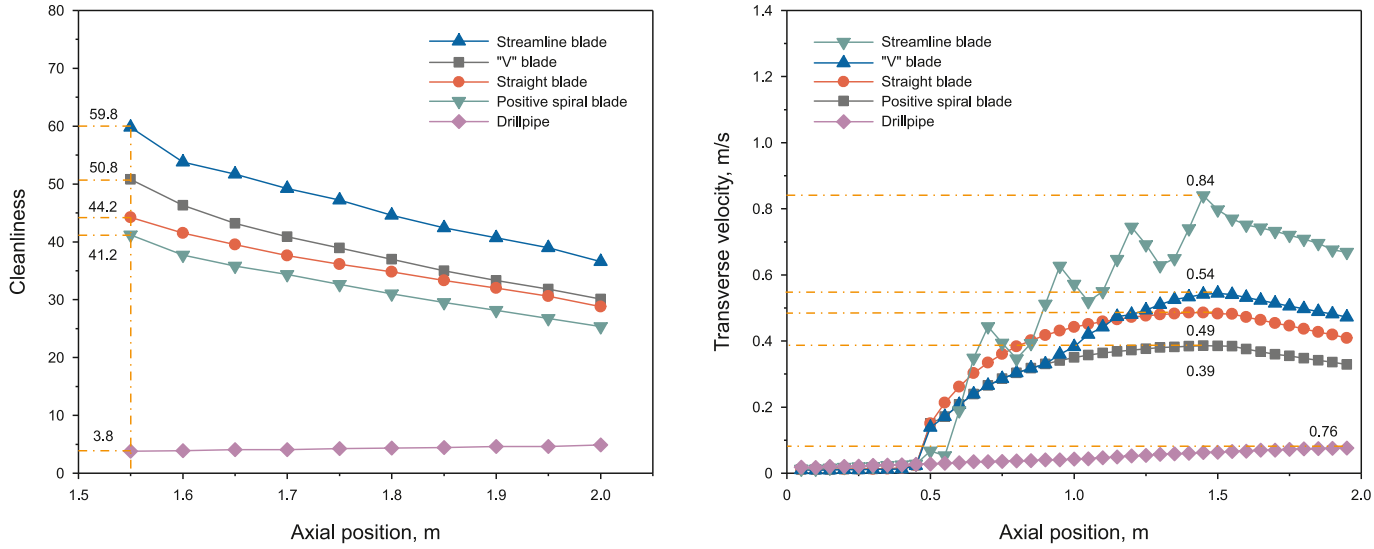

(a) Variation of the wellbore cleanliness **(b)** Variation of the transverse velocity

Fig. 15. Cleanliness and transverse velocity of four types of removers at: ROP = 40 m/h, ω_d = 120 rpm, v = 35 L/s, D_h = 215.9 mm, e = 0, τ_0 = 5 Pa, K = 0.1 Pa·s^n, n = 0.5.

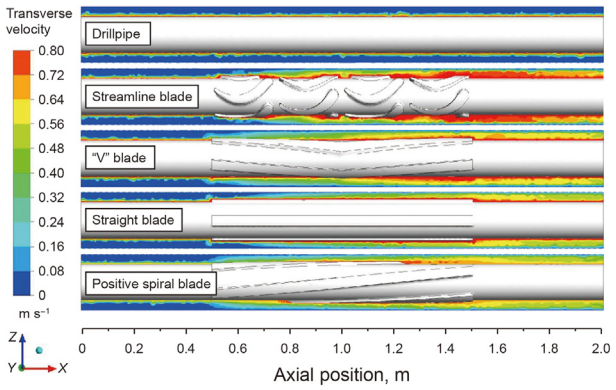

Fig. 16. Transverse velocity distribution under different removers at: ROP = 40 m/h, ω_d = 120 rpm, v = 35 L/s, D_h = 215.9 mm, e = 0, τ_0 = 5 Pa, K = 0.1 Pa·s^n, n = 0.5.

3.4.3. *Effect of rate of penetration*

Fig. 19(a) and (b) show the wellbore cleanliness and transverse velocity at varied rates of penetration.

Fig. 19(a) shows that the increase of ROP results in a sharp decline in the wellbore cleanliness. The cleanliness decreases from 86.3 to 46.9 as the ROP increases from 30 to 50 m/h. This is because as the drill bit cuts through the formation, it produces an increasing amount of cuttings. These cuttings contribute to both the volume fraction and the height of the cutting bed that accumulates in the annulus. Furthermore, an increased concentration of cuttings results in additional drag and inter-particle frictional forces, which can decrease the kinetic energy and movement speed of the cutting particles.

The transverse velocity is almost unchanged with the ROP increase due to the drillpipe rotational speed and the fluid flow rate holding constant, as shown in Fig. 19(b). Considering that the transverse velocity of the drilling fluid plays a crucial role in hole

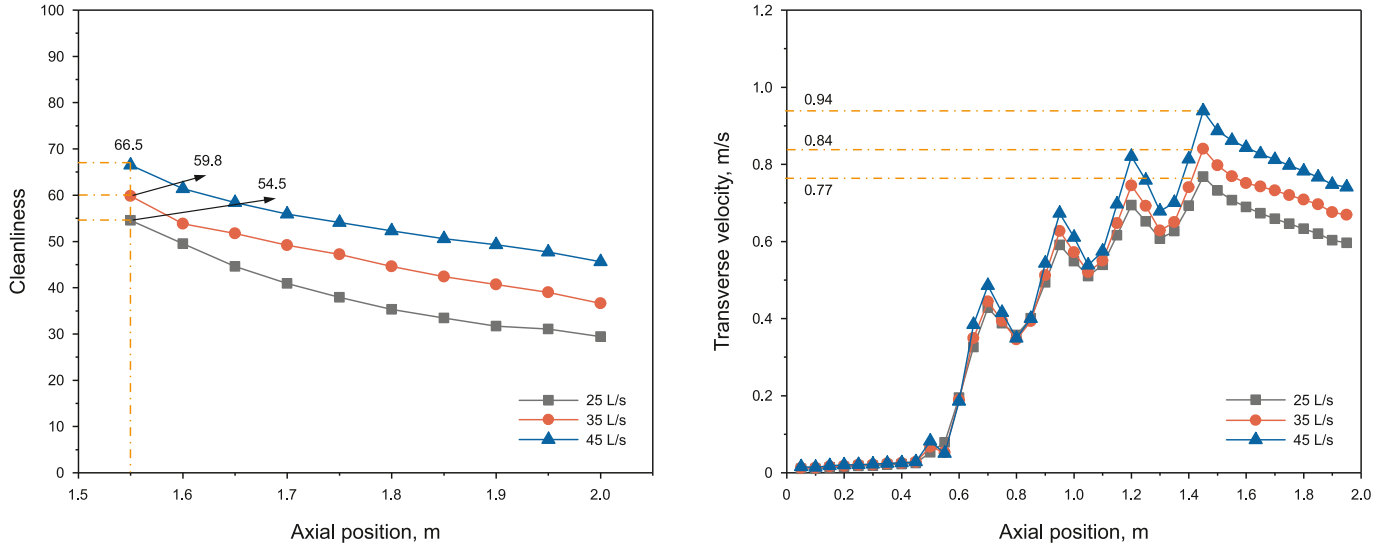

(a) Variation of wellbore cleanliness **(b)** Variation of transverse velocity

Fig. 17. Effect of drilling fluid flow rate on wellbore cleanliness and transverse velocity at: ROP = 40 m/h, ω_d = 120 rpm, D_h = 215.9 mm, e = 0, τ_0 = 5 Pa, K = 0.1 Pa·s^n, n = 0.5.

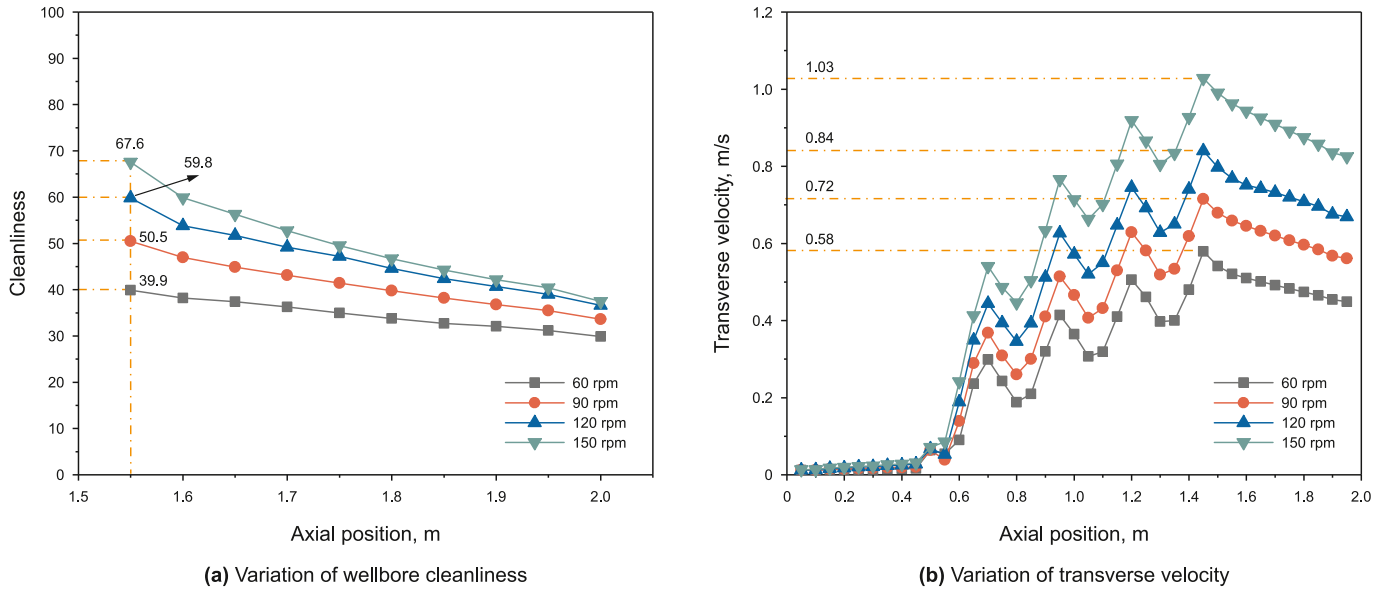

(a) Variation of wellbore cleanliness **(b)** Variation of transverse velocity

Fig. 18. Effect of drillpipe rotational speed on wellbore cleanliness and transverse velocity at: ROP = 40 m/h, v = 35 L/s, D_h = 215.9 mm, e = 0, τ_0 = 5 Pa, K = 0.1 Pa·s^n, n = 0.5.

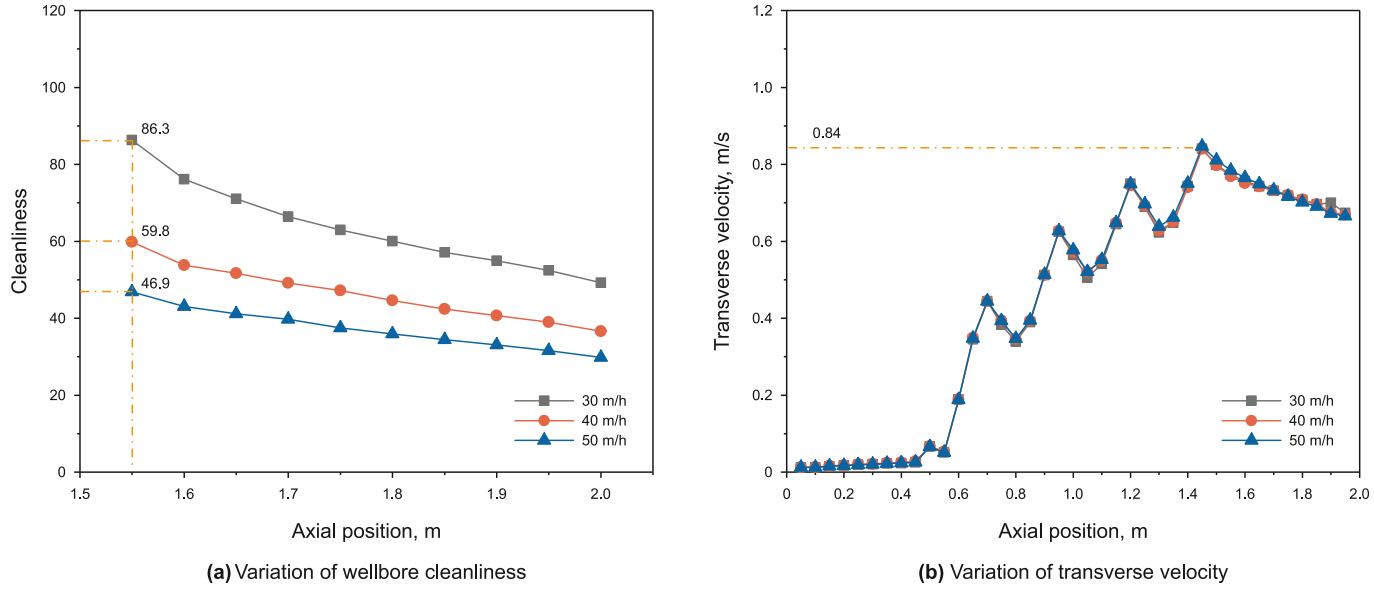

(a) Variation of wellbore cleanliness **(b)** Variation of transverse velocity

Fig. 19. Effect of ROP on wellbore cleanliness and transverse velocity at: ω_d = 120 rpm, v = 35 L/s, D_h = 215.9 mm, e = 0, τ_0 = 5 Pa, K = 0.1 Pa·s^n, n = 0.5.

cleaning, the flow rate or drill pipe rotational speed can be reasonably raised to restrain the deduction of remover's cleaning capacity due to higher ROP.

3.4.4. Effect of wellbore size

To investigate the difference in cuttings removal effect of the remover under different wellbore sizes, wellbore sizes of 8½", 12¼", and 17½" were selected to conduct numerical simulations. According to the engineering practice, the corresponding flow rate of drilling fluid was set as 35, 50, and 65 L/s, respectively, and cuttings bed removers of the same size were employed in three different wellbore dimensions. The variation of the wellbore cleanliness and transverse velocity at different wellbore sizes are shown in Fig. 20.

Fig. 20(a) shows that the cleanliness of 8½" is approximately 3 times that of 17½" section or 2 times that of 12¼" section. The maximum transverse velocity decreases from 1.55 to 0.21 m/s as the wellbore size increases from 8½" to 17½", as seen in Fig. 20(b). This is because holding the ROP constant and increasing the wellbore size can generate more cuttings simultaneously. In addition, the flow rate in the annulus is seriously weakened due to the larger wellbore size. Consequently, the wellbore cleanliness and the transverse velocity of drilling fluid are drastically declined.

Fig. 21 illustrates the transverse velocity distribution of fluid fields in different wellbore sizes. Under the action of removers, the transverse velocity component of fluid is significantly increased, especially for 8½" wellbore. The central region of the fluid field near the remover exhibits the highest transverse velocity, which decreases rapidly as the distance from the remover increases, mainly due to the viscosity of the drill fluid. Furthermore, the transverse velocity near the wellbore wall is close to zero owing to the wall viscosity effect.

The results indicate it is more difficult to clean the large

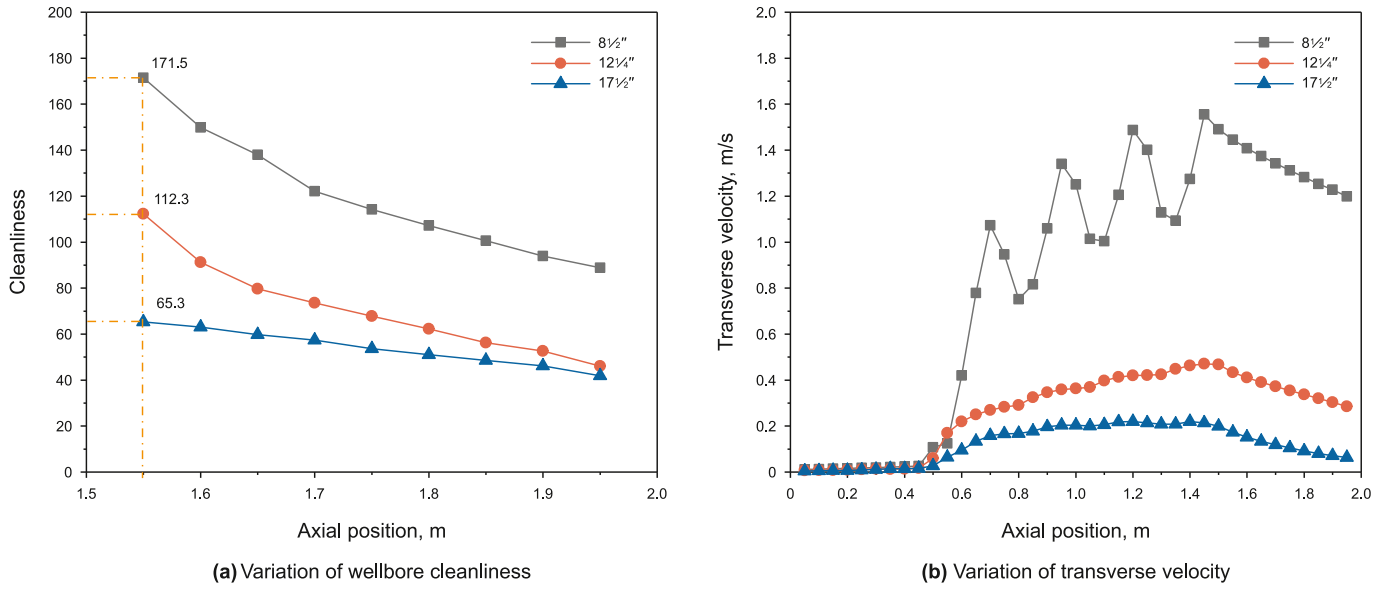

Fig. 20. Effect of wellbore size on wellbore cleanliness and transverse velocity at: ROP = 40 m/h, ω_d = 120 rpm, e = 0, τ_0 = 5 Pa, K = 0.1 Pa·s^n, n = 0.5.

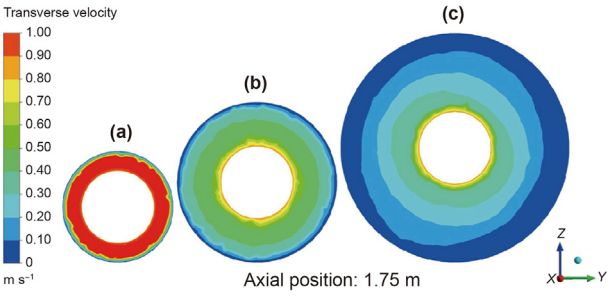

Fig. 21. Effect of wellbore size on transverse velocity distribution at τ_0 = 5 Pa, K = 0.1 Pa·s^n, n = 0.5, e = 0. (**a**) ROP = 40 m/h, ω_d = 120 rpm, v = 35 L/s, D_h = 215.9 mm. (**b**) ROP = 40 m/h, ω_d = 120 rpm, v = 50 L/s, D_h = 311.15 mm. (**c**) ROP = 40 m/h, ω_d = 120 rpm, v = 65 L/s, D_h = 411.5 mm.

wellbore than the smaller one. The reason is that the larger wellbore usually means a lower drilling fluid flow rate and a relatively minor action range of remover. Thus, to optimize the structure of the remover and enhance the transverse velocity of the fluid field, it is advisable to increase the radial contact area of the blade.

3.4.5. *Effect of drilling fluid rheology*

Drilling fluid rheological properties play a crucial role in the transportation of cuttings (Gulraiz and Gray, 2020). The properties of the drilling fluids (Table 1) used in this study were adapted from the work of Wang et al. (2022).

The H–B model comprises three key rheological parameters, namely, the consistency coefficient (K), flow behavior index (n), and yield stress (τ_0). However, in the investigation of drilling fluid rheology, changing only one rheological parameter while keeping the other two fixed can be challenging. In drilling engineering, the most commonly utilized rheological testing instrument is the six-speed rotating viscometer. Some drilling engineers have used the viscometer dial readings directly instead of rheological parameters (Ramsey, 2019). Several studies have indicated that the 6 rpm Fann dial reading of drilling fluid is a crucial factor influencing flow characteristics and hydraulic performance (Mahmoud et al., 2020).

For Fann rotational viscometers, the 6 rpm Fann dial reading θ_6 is defined as follows (Wang et al., 2022):

$$\theta_6 = \frac{1}{0.511}\left(\tau_0 + 10.21^n K\right) \tag{10}$$

Fig. 22 illustrates the distribution of cuttings volume fraction under five 6 rpm Fann dial readings. At low 6 rpm Fann dial readings, the cuttings tend to settle at the lower annulus. However, as the 6 rpm Fann dial reading θ_6 increases from 1.26 to 39.45, the maximum cuttings volume fraction significantly decreases, leading to a more even distribution of cuttings within the annulus. The reason for this is that a lower 6 rpm Fann dial reading indicates a lower shear viscosity of the drilling fluid. As a result, cuttings settle more easily due to less viscous force. However, when the 6 rpm Fann dial reading increases to a critical value of approximately 30, the viscosity of the drilling fluid is high enough to overcome gravity and transport cuttings to the upper high-velocity zone, causing them to distribute evenly in the annulus. Continue to increase the 6 rpm fan dial reading θ_6, i.e., the shear viscosity of the drilling fluid has almost no effect on the maximum cuttings concentration.

Fig. 23 illustrates the effect of fluid rheology on wellbore cleanliness. The graph demonstrates that as the 6 rpm Fann dial reading θ_6 increases, the cleanliness of the cuttings bed remover also increases, particularly at lower θ_6 values. However, after reaching a certain value of θ_6, the cleanliness no longer shows a significant increase.

3.4.6. *Effect of eccentricity*

Although many methods have been used to maintain the center of the drillpipe, eccentricity is still inevitable, especially in extended-reach or long-horizontal wells. Four different eccentricities were simulated to analyze the cuttings transport behavior in a horizontal well, as shown in Figs. 24–26.

As evident from Fig. 24(a)–(d), an increase in eccentricity leads to a noticeable rise in the transverse velocity of the lower annulus, accompanied by a sharp decline in the upper annulus velocity. As the eccentricity increases from 0 to 0.5, the region with high transverse velocity gradually shifts downward towards the lower annulus, and the area with the highest velocity increasingly concentrates on the narrow gap region. Therefore, the cuttings bed remover forces fluid deflection, which tangentially drags cuttings with the drilling fluid, causing more cuttings to move from the

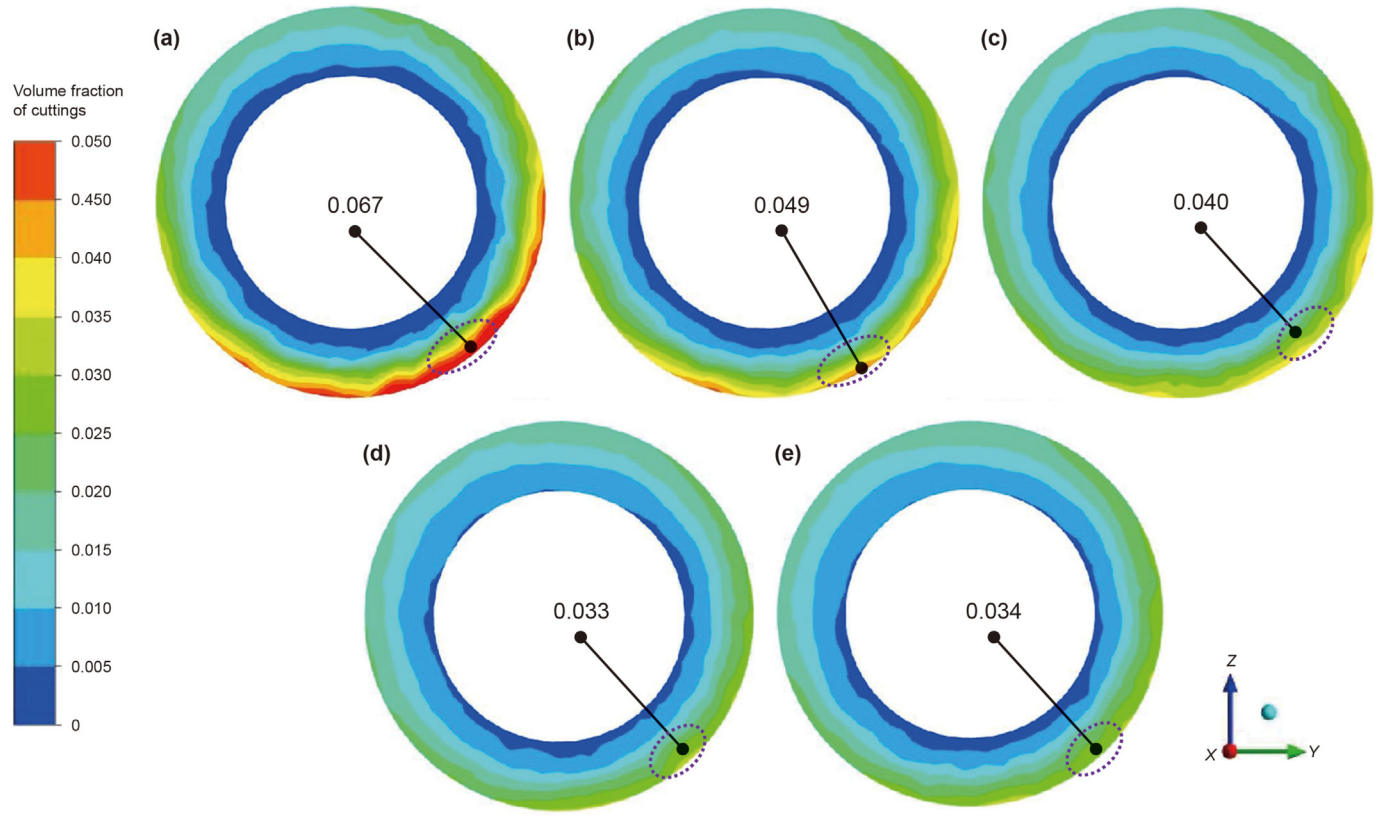

Fig. 22. Effect of fluid rheology on distribution patterns of cuttings volume fraction at: ROP = 40 m/h, v = 35 L/s, ω_d = 120 rpm, D_h = 215.9 mm, e = 0. (**a**) θ_6 = 1.26; (**b**) θ_6 = 10.18; (**c**) θ_6 = 20.07; (**d**) θ_6 = 29.66; (**e**) θ_6 = 39.45.

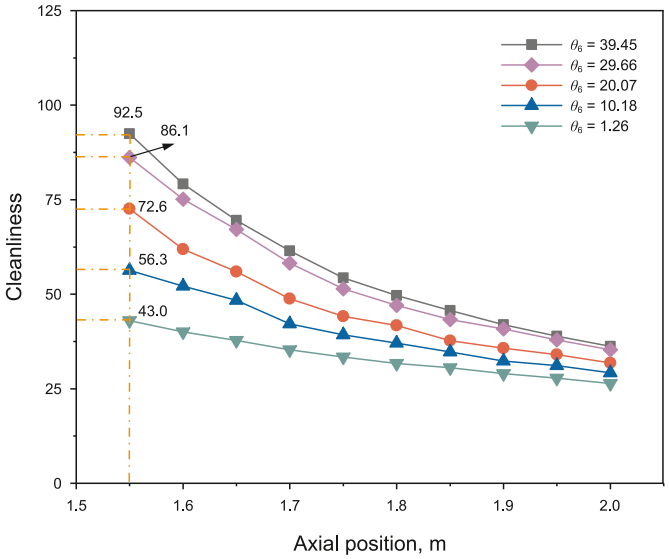

Fig. 23. Effect of fluid rheology on wellbore cleanliness at: ROP = 40 m/h, ω_d = 120 rpm, D_h = 215.9 mm, e = 0. (**a**) θ_6 = 1.26; (**b**) θ_6 = 10.18; (**c**) θ_6 = 20.07; (**d**) θ_6 = 29.66; (**e**) θ_6 = 39.45.

bottom of the annulus to the dispersed layer. The concentration distribution of cuttings is depicted in Fig. 25(a)–(d). It can be predicted that the increase in transverse velocity resulting from the eccentricity increase has a positive effect on hole cleaning, this is consistent with the prediction of cleanliness, as shown in Fig. 26.

4. Case study

Take an extended-reach well X1 in the South China Sea as an example. The total well depth is 5266 m, the vertical depth is 1218.80 m, the horizontal displacement is 4636.37 m, and the horizontal displacement-vertical depth ratio reaches 3.8. The projection of the wellbore trajectory curve is illustrated in Fig. 27.

According to the previous operation experience in this oilfield, it is usually difficult for drilling cuttings to transport to the surface. Due to pipe sticking caused by cuttings bed, a lot of drilling time is wasted. Thus, installing removers to properly enhance the transport of cuttings is necessary.

The average volume fraction of cuttings on the cross-section can be used to represent the number of cuttings in the annulus. A smaller volume fraction of cuttings indicates better performance of cuttings transport. Generally, the volume fraction of cuttings increases with the distance from the remover, and if the volume fraction in the annulus exceeds 5%, pipe sticking is prone to occur (Li and Liu, 1994). The removers need to be installed at certain spacings.

4.1. Effect of parameters on the installation spacing of removers

4.1.1. Effect of drilling fluid flow rate

Based on the input parameters listed in Table 1, the optimal installation spacings were calculated at different flow rates, as shown in Fig. 28. The axial position in the figure means the distance away from the remover along the wellbore axis. The ordinates in Fig. 28 specifically refer to the average volume fraction of the entire annulus.

Fig. 28 shows that the recommended installation spacings are 9,

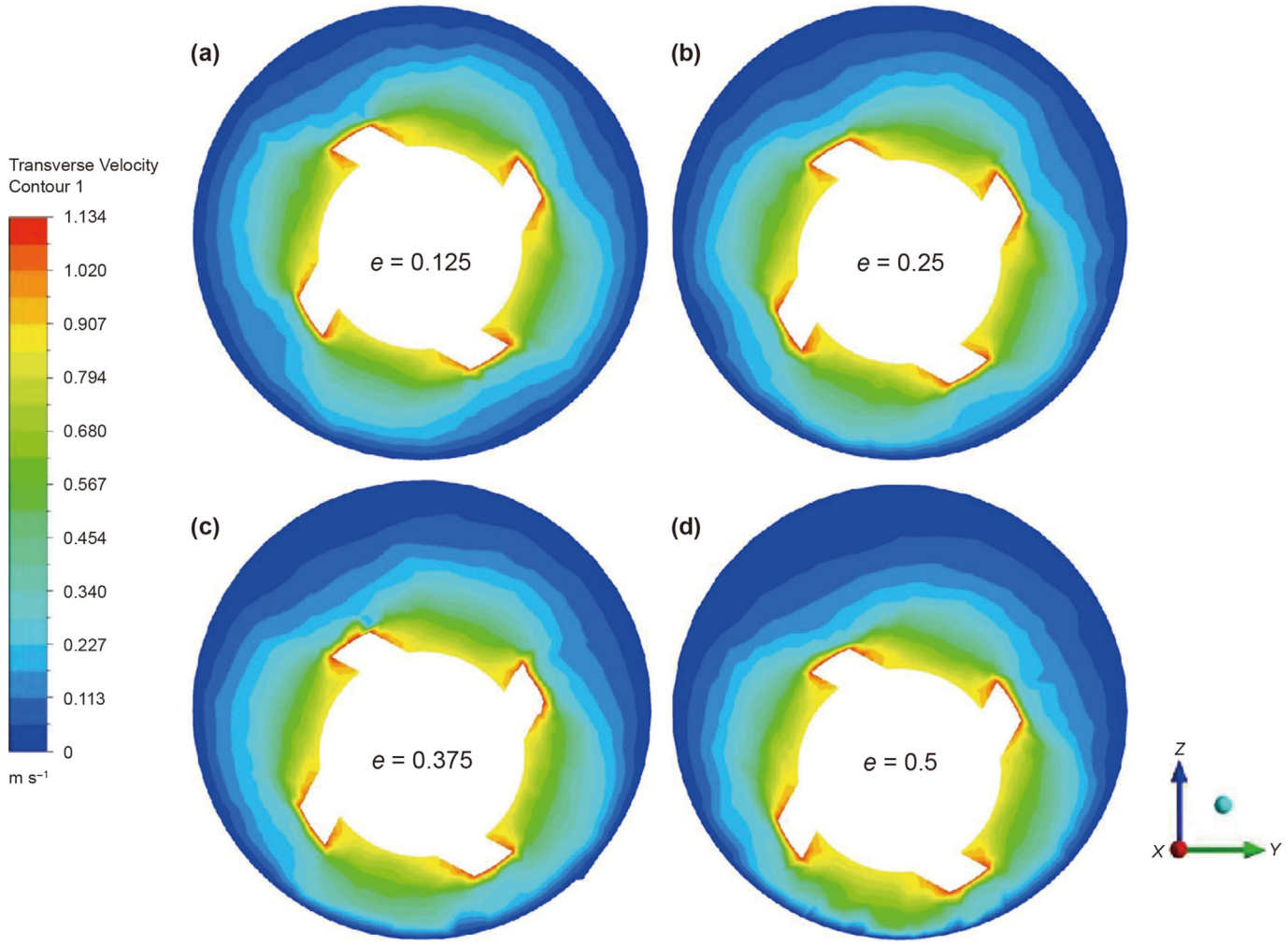

Fig. 24. Effect of eccentricity on transverse velocity at: v = 35 L/s, ROP = 40 m/h, ω_d = 120 rpm, D_h = 311.15 mm, τ_0 = 5 Pa, K = 0.1 Pa·s^n, n = 0.5.

17 and 25 drillpipes when the flow rates are 40, 50 and 60 L/s. Therefore, there is no need to install removers. A greater flow rate contributes to accelerating the speed of the cuttings moving towards the outlet alleviating the cuttings deposition rate. However, the excessive flow rate of drilling fluid may destroy wellbore stability and increase the annular pressure loss a lot. Therefore, the installation spacings need to be optimized under reasonable working conditions to improve cutting transport efficiency.

4.1.2. Effect of drillpipe rotational speed

Fig. 29 shows that the optimal installation spacing of removers is decreased with the increase in rotational speed of the drillpipe. When the rotational speeds are 40, 80 and 120 rpm, the optimum installation spacings are 3, 6, and 17 drillpipes. Pipe rotation produces centrifugal forces acting on the cutting particles, and then the accumulated cuttings are evenly distributed in the annulus. Therefore, the high rotational speed of drillpipe contributes to decreasing the thickness of cuttings bed and improving the performance of cuttings transport.

4.1.3. Effect of rate of penetration

Fig. 30 shows that the optimal installation spacing of removers decreases with the increase of ROP. The recommended installation spacings are 17, 13, and 8 drillpipes when the ROPs are 30, 40 and 50 m/h. As the ROP increases, more cutting particles need to be carried out in time. Otherwise, the cuttings concentration will rapidly reach the critical thickness of cuttings bed. Then, smaller installation spacing needs to be adopted to remove the accumulated cuttings.

4.1.4. Effect of wellbore size

Fig. 31 shows the variations of the cuttings concentration in the annulus of 8½", 12¼", and 17½" wellbores. The cuttings concentration in the 8½" section keeps a stable value of about 1% as the distance from the remover increases. Then, there is no need to install removers because the cuttings concentration is lower than the threshold value, namely 5%.

The optimal installation spacing for the 17½" well section is relatively small, only 2 drill pipes. Therefore, it is recommended to properly enhance the drilling parameters and select the remover

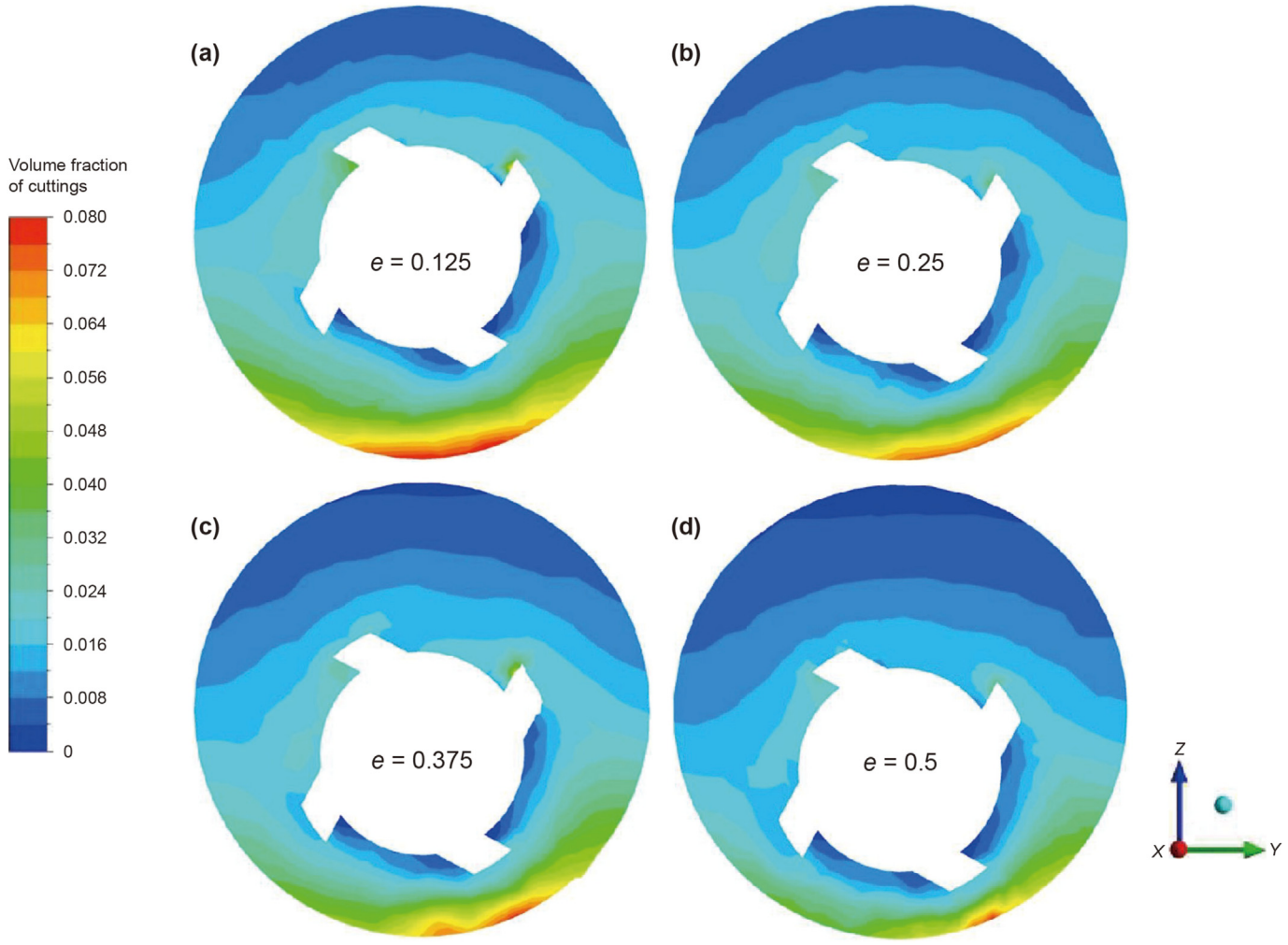

Fig. 25. Effect of eccentricity on distribution patterns of cuttings volume fraction at: v = 35 L/s, ROP = 40 m/h, ω_d = 120 rpm, D_h = 311.15 mm, τ_0 = 5 Pa, K = 0.1 Pa·s^n, n = 0.5.

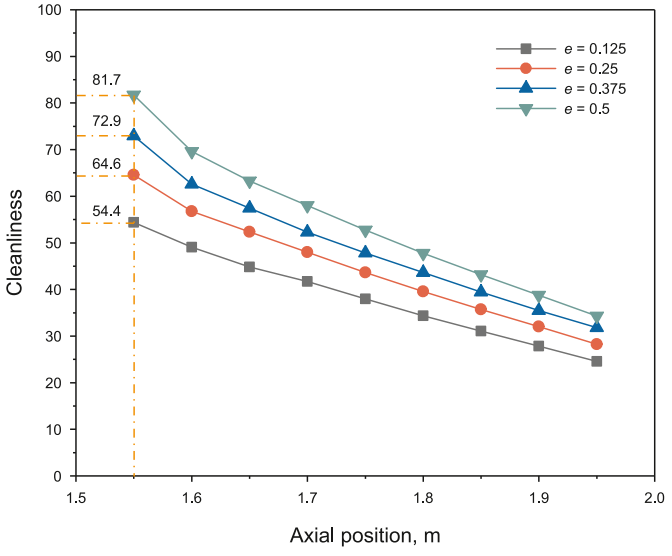

Fig. 26. Effect of eccentricity on wellbore cleanliness at: v = 35 L/s, ROP = 40 m/h, ω_d = 120 rpm, D_h = 311.15 mm, τ_0 = 5 Pa, K = 0.1 Pa·s^n, n = 0.5.

with better performance for hole cleaning.

Overall, removers are not recommended for 8½" section, and the recommended installation spacings are 17 and 2 drill pipes for 12¼" and 17½" sections.

4.2. Field results

When well X1 drills to 970 m, the cuttings transported to the surface were greatly reduced, and the excessive value of hook load increased to 140 kN. The probable reason is that cuttings accumulated in this section. According to the calculation results, the installation scheme of removers is given as follows.

(1) In the 12¼" hole section, removers are installed with the spacing of 17 drill pipes (about 170 m).
(2) In the 17½" hole section, removers are installed with the spacing of 2 drill pipes (about 20 m).

After installing the removers in well X1, it can be observed from the shale shake that the amount of returned cuttings was significantly increased. Meanwhile, the torque on the drill string was remarkably reduced.

Generally, inefficient hole cleaning leads to back-pressure. Thus,

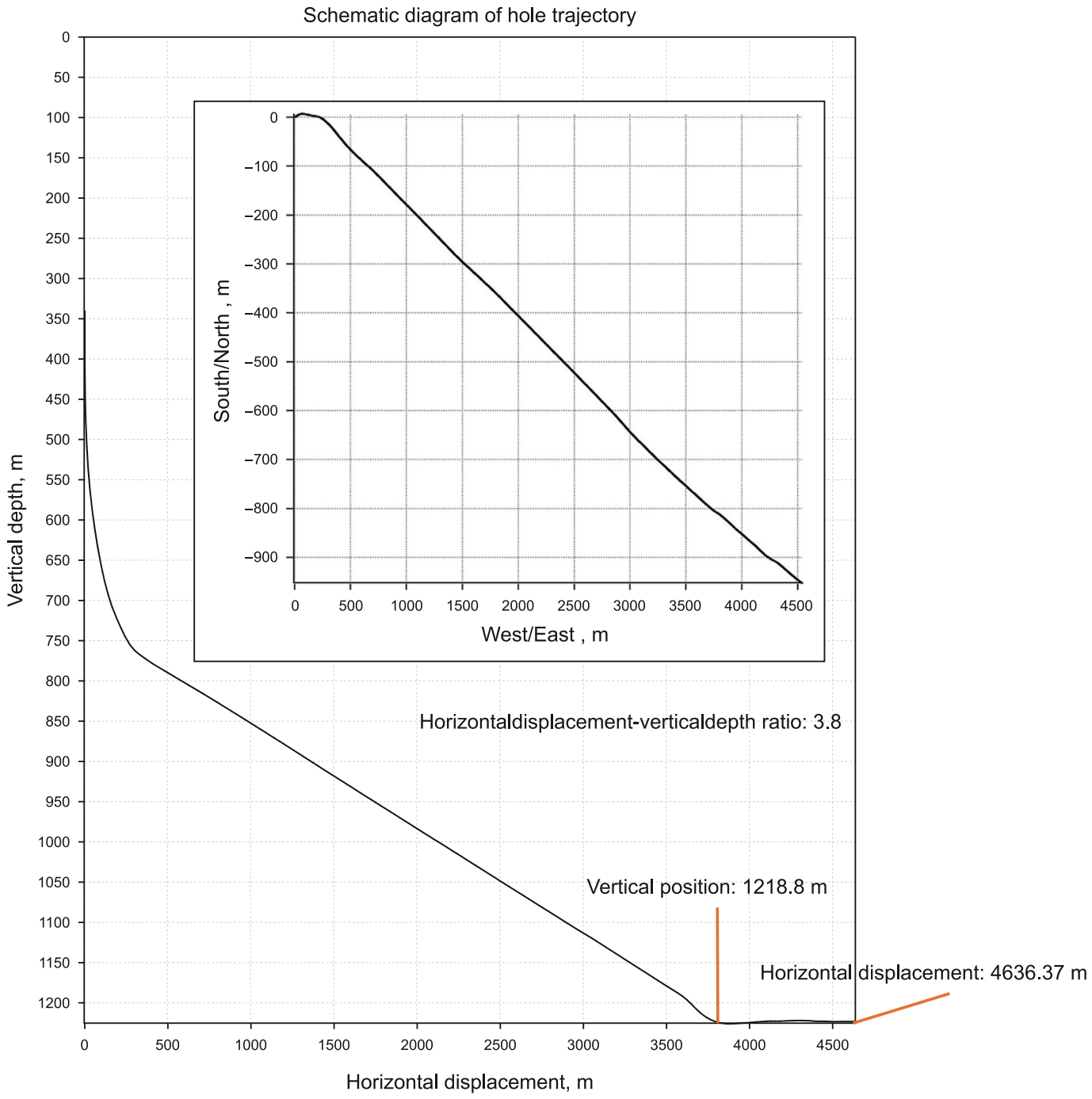

Fig. 27. Wellbore trajectory curve projection.

to further clarify the quality of hole cleaning, the back-pressure of three wells, including well X1, well X2, and well X3 are obtained and reported in Table 4. The three wells are located in the same block with similar well conditions, while removers were adopted in well X1. Compared with the data of adjacent wells, the starting depth of back-pressure of well X1 is considerably deepened, and the maximum back-pressure difference is significantly reduced.

The field application results demonstrate that the removers play a vital role in hole cleaning, and the calculation method of the installation spacing is reasonable.

5. Conclusion

In this paper, a cuttings transport model of the cuttings bed remover was developed based on the Eulerian-Eulerian two-phase flow model and dynamic mesh technology. The accuracy of the model was validated using experimental data. The main conclusions drawn from the study are as follows.

1. The blade structure of remover is closely related to wellbore cleanliness, the cuttings transport capacity can be improved by

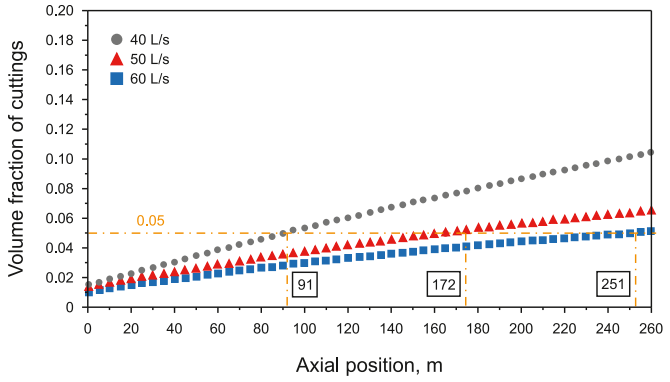

Fig. 28. Effect of drilling fluid flow rate on the volume fraction of cuttings at: ROP = 30 m/h, ω_d = 120 rpm, D_h = 311.15 mm, e = 0.2, τ_0 = 5 Pa, K = 0.8 Pa·s^n, n = 0.5.

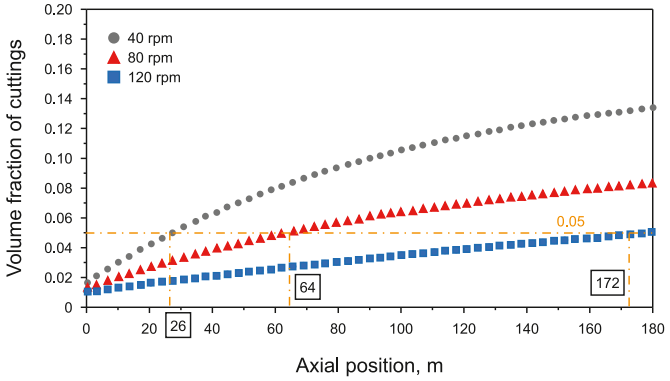

Fig. 29. Effect of drilling fluid flow rate on the volume fraction of cuttings at: ROP = 30 m/h, v = 50 L/s, D_h = 311.15 mm, e = 0.2, τ_0 = 5 Pa, K = 0.8 Pa·s^n, n = 0.5.

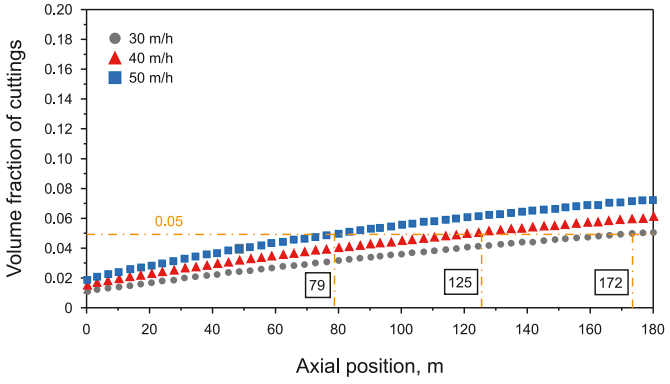

Fig. 30. Effect of ROP on the volume fraction of cuttings at: ω_d = 120 rpm, v = 50 L/s, D_h = 311.15 mm, e = 0.2, τ_0 = 5 Pa, K = 0.8 Pa·s^n, n = 0.5.

optimizing the blade shape. Due to the unique geometrical characteristics increasing fluid velocity and excellent vortex generation capability, the streamline blade presents the best performance followed by "V" blade and straight blade, and the hole cleaning performance of positive spiral blade is the worst.

2. Increasing drilling fluid flow rate can significantly improve the performance of the new remover. Whereas the increase in wellbore size or penetration rate shows a considerably adverse impact on the cuttings removal. The results are consistent with previous studies. It is proved that cleanliness can provide a good prediction of the performance of cuttings bed remover.
3. The performance of the cuttings bed remover improves as the rotational speed increases, but there is a threshold above which further increases in rotation speed do not result in a significant improvement.
4. The 6 rpm Fann dial reading θ_6 was used to comprehensively evaluate the effects of the Herschel-Bulkley model rheological parameters on the performance of cuttings bed remover. A higher θ_6 is beneficial up to a certain threshold value, beyond which it does not significantly improve the performance.
5. Increasing the eccentricity of the cutting bed remover can mitigate the accumulation of cuttings. As the eccentricity increases, the region with high transverse velocity gradually shifts to the lower annulus. This promotes the suspension and transportation of cuttings, ultimately improving the hole cleaning performance of the cutting bed remover.
6. Based on the CFD mathematical model, the reasonable installation spacings at different drilling parameters were obtained and applied to the field. The effectiveness of the cuttings bed remover in eliminating cuttings bed was verified by comparing the back-pressure with adjacent wells. It is worth noting that this may not conclusively determine the most optimal installation spacing for the remover developed.
7. The cuttings were assumed mono-sized spherical geometries. However, during drilling, cuttings actually possess irregular shapes and exhibit a high degree of dispersion. Considering these factors is beneficial to obtain more accurate numerical simulation results. The future direction of this study will focus on the investigation of the effects of cuttings shape and size on the cuttings transport.

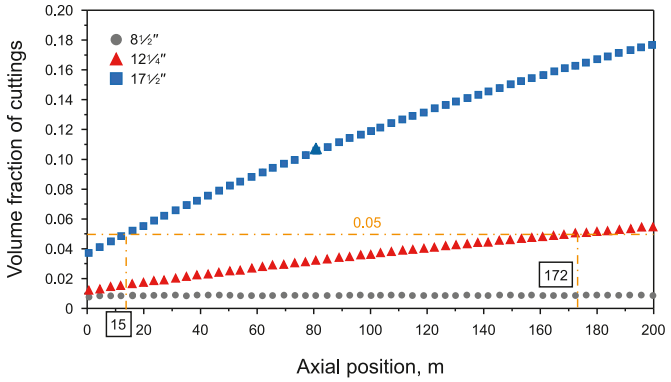

Fig. 31. Volume fraction of cuttings variation chart at different wellbore sizes at τ_0 = 5 Pa, K = 0.8 Pa·s^n, n = 0.5, e = 0.2. (**a**) ROP = 30 m/h, ω_d = 120 rpm, v = 35 L/s. (**b**) ROP = 30 m/h, ω_d = 120 rpm, v = 50 L/s, D_h = 311.15 mm. (**c**) ROP = 20 m/h, ω_d = 20 rpm, v = 50 L/s, D_h = 444.5 mm.

Table 4
Statistics of back-pressure of well X1, well X2, and well X3.

Wells	Starting depth of back-pressure, m	Maximum back-pressure, klb	Difference of back-pressure, klb
X1	2814	27	15
X2	2054	40	26
X3	2030	35	22

CRediT authorship contribution statement

Shuo Peng: Writing – original draft, Software, Methodology, Conceptualization. **Wen-Jun Huang:** Writing – review & editing, Validation, Conceptualization. **De-Li Gao:** Writing – review & editing, Supervision, Conceptualization.

Declaration of competing interest

We declare that we do not have any commercial or associative interest that represents a conflict of interest in connection with the work submitted.

Acknowledgments

The authors gratefully acknowledge the financial support from the Natural Science Foundation of China (Grant Nos. 52222401, 52234002, 52394250, 52394255), Science Foundation of China University of Petroleum, Beijing (Grant No. ZXZX20230083), and other projects (ZLZX2020-01-07-01). The authors also gratefully acknowledge the computing resources provided by Hefei advanced computing center.

References

Amanna, B., Movaghar, M.R.K., 2016. Cuttings transport behavior in directional drilling using computational fluid dynamics (CFD). J. Nat. Gas Sci. Eng. 34, 670–679. https://doi.org/10.1016/j.jngse.2016.07.029.

Araoye, A.A., Badr, H.M., Ahmed, W.H., 2017. Investigation of flow through multi-stage restricting orifices. Ann. Nucl. Energy 104, 75–90. https://doi.org/10.1016/j.anucene.2017.02.002.

Awad, A.M., Hussein, I.A., Nasser, M.S., et al., 2022. A CFD-RSM study of cuttings transport in non-Newtonian drilling fluids: impact of operational parameters. J. Petrol. Sci. Eng. 208, 109613. https://doi.org/10.1016/j.petrol.2021.109613.

Bilgesu, H.I., Mishra, N., Ameri, S., 2007. Understanding the effects of drilling parameters on hole cleaning in horizontal and deviated wellbores using computational fluid dynamics. In: Eastern Regional Meeting. https://doi.org/10.2118/111208-MS.

Boulet, J.G., Shepherd, J.A., Batham, J., et al., 2000. Improved hole cleaning and reduced rotary torque by new external profile on drilling equipment. In: IADC/SPE Drilling Conference. https://doi.org/10.2118/59143-MS.

Brett, J.F., Beckett, A.D., Holt, C.A., et al., 1989. Uses and limitations of drillstring tension and torque models for monitoring hole conditions. SPE Drill. Eng. 4 (3), 223–229. https://doi.org/10.2118/16664-PA.

Busch, A., Johansen, S.T., 2020. Cuttings transport: on the effect of drill pipe rotation and lateral motion on the cuttings bed. J. Petrol. Sci. Eng. 191, 107136. https://doi.org/10.1016/j.petrol.2020.107136.

Cao, T., Yu, K., Chen, X.Y., et al., 2019. Numerical investigations on the effect of a cuttings bed remover on the cuttings carrying capacity in horizontal drilling. In: Proceedings of ASME 2019 Pressure Vessels & Piping Conference. https://doi.org/10.1115/PVP2019-93809.

Chen, X.Y., Gao, D.L., Guo, B.Y., 2016. A method for optimizing jet-mill-bit hydraulics in horizontal drilling. SPE J. 21 (2), 416–422. https://doi.org/10.2118/178436-PA.

Cho, H., Shah, S.N., Osisanya, S.O., 2002. A three-segment hydraulic model for cuttings transport in coiled tubing horizontal and deviated drilling. J. Can. Pet. Technol. 41 (6). PETSOC-02-06-03. https://doi.org/10.2118/02-06-03.

Duan, M.Q., Miska, S., Yu, M.J., et al., 2008. Transport of small cuttings in extended reach drilling. SPE Drill. Complet. 23 (3), 258–265. https://doi.org/10.2118/104192-MS.

Ford, J.T., Peden, J.M., Oyeneyin, M.B., et al., 1990. Experimental investigation of drilled cuttings transport in inclined boreholes. In: SPE Annual Technical Conference and Exhibition. https://doi.org/10.2118/20421-MS.

Gulraiz, S., Gray, K.E., 2020. Investigating the effects of plug viscosity on annular pressure drop and cuttings transport in a concentric annulus. J. Nat. Gas Sci. Eng. 76, 103210. https://doi.org/10.1016/j.jngse.2020.103210.

Heydari, O., Sahraei, E., Skalle, P., 2017. Investigating the impact of drillpipe's rotation and eccentricity on cuttings transport phenomenon in various horizontal annuluses using computational fluid dynamics (CFD). J. Petrol. Sci. Eng. 156, 801–813. https://doi.org/10.1016/j.petrol.2017.06.059.

Hovda, S., 2019. Optimal procedures for lowering and applying weight on the bit when starting to drill. J. Petrol. Sci. Eng. 174, 872–879. https://doi.org/10.1016/j.petrol.2018.11.034.

Huque, M.M., Butt, S., Zendehboudi, S., et al., 2020. Systematic sensitivity analysis of cuttings transport in drilling operation using computational fluid dynamics approach. J. Nat. Gas Sci. Eng. 81, 103386. https://doi.org/10.1016/j.jngse.2020.103386.

Li, H.Q., Liu, X.S., 1994. Determination method of reasonable annular velocity in horizontal well drilling. J. China Univ. Pet., Ed. Nat. Sci. 18 (5), 27–31. CNKI:SUN:SYDX.0.1994-05-004 (in Chinese).

Li, J., Walker, S., 2001. Sensitivity analysis of hole cleaning parameters in directional wells. SPE J. 6 (4), 356–363. https://doi.org/10.2118/74710-PA.

Lockett, T.J., Richardson, S.M., Worraker, W.J., 1993. The importance of rotation effects for efficient cuttings removal during drilling. In: SPE/IADC Drilling Conference. https://doi.org/10.2118/25768-MS.

Mahmoud, H., Hamza, A., Nasser, M.S., et al., 2020. Hole cleaning and drilling fluid sweeps in horizontal and deviated wells: comprehensive review. J. Petrol. Sci. Eng. 186, 106748. https://doi.org/10.1016/j.petrol.2019.106748.

Miao, H., Qiu, Z., Dokhani, V., et al., 2023. Numerical modeling of transient cuttings transport in deviated wellbores. Geoenergy Sci. Eng., 211875 https://doi.org/10.1016/j.geoen.2023.211875.

Nguyen, D., Rahman, S.S., 1996. A three-layer hydraulic program for effective cuttings transport and hole cleaning in highly deviated and horizontal wells. In: SPE/IADC Asia Pacific Drilling Technology. https://doi.org/10.2118/36383-MS.

Ofei, T.N., Irawan, S., Pao, W., 2015. Drilling parameter effects on cuttings transport in horizontal wellbores: a review. ICIPEG 2014, 199–207. https://doi.org/10.1007/978-981-287-368-2_18.

Pang, B.X., Wang, S.Y., Lu, C.L., et al., 2019. Investigation of cuttings transport in directional and horizontal drilling wellbores injected with pulsed drilling fluid using CFD approach. Tunn. Undergr. Space Technol. 90, 183–193. https://doi.org/10.1016/j.tust.2019.05.001.

Ramadan, Ahmed, Munawar, et al., 2011. Experimental studies on the effect of mechanical cleaning devices on annular-cuttings concentration. J. Petrol. Technol. 63 (2), 45–46. https://doi.org/10.2118/134269-MS.

Ramsey, M.S., 2019. Practical Wellbore Hydraulics and Hole Cleaning: Unlock Faster, More Efficient, and Trouble-free Drilling Operations. Gulf Professional Publishing.

Rishi, B.A., Stefan, M., Ergun, K., et al., 2000. Selecting drilling fluid properties and flow rates for effective hole cleaning in high-angle and horizontal wells. In: SPE Annual Technical Conference and Exhibition. https://doi.org/10.2118/63050-MS.

Rooki, R., Ardejani, F.D., Moradzadeh, et al., 2015. CFD simulation of rheological model effect on cuttings transport. J. Dispersion Sci. Technol. 36 (3), 402–410. https://doi.org/10.1080/01932691.2014.896219.

Saasen, A., 1998. Hole cleaning during deviated drilling-The effects of pump rate and rheology. In: SPE Europec Featured at EAGE Conference and Exhibition. https://doi.org/10.2118/50582-MS.

Siruvuri, C., Nagarakanti, S., Samuel, R., 2006. Stuck pipe prediction and avoidance: a convolutional neural network approach. In: IADC/SPE Drilling Conference. https://doi.org/10.2118/98378-MS.

Sun, B.J., Xiang, H.F., Li, H., et al., 2017. Modeling of the critical deposition velocity of cuttings in an inclined-slimhole annulus. SPE J. 22 (4), 1213–1224. https://doi.org/10.2118/185168-PA.

Sun, X., Wang, K., Yan, T., et al., 2014. Effect of drillpipe rotation on cuttings transport using computational fluid dynamics (CFD) in complex structure wells. J. Pet. Explor. Prod. Technol. 4, 255–261. https://doi.org/10.1007/s13202-014-0118-x.

Van Puymbroeck, L., 2013. Increasing drilling performance using hydro-mechanical hole cleaning devices. In: SPE Unconventional Gas Conference and Exhibition. https://doi.org/10.2118/164005-MS.

Van Puymbroeck, L., El Bachiri, K., 2013. New generation drill pipe to increase drilling performance in ERD wells. In: SPE/IADC Middle East Drilling Technology Conference & Exhibition. https://doi.org/10.2118/166775-MS.

Van Puymbroeck, L., Williams, H., 2013. Increasing drilling performance in ERD wells with new generation drill pipe. In: Unconventional Resources Technology Conference, pp. 1060–1070. https://doi.org/10.1190/urtec2013-108.

Van Wachem, B.G.M., Almstedt, A.E., 2003. Methods for multiphase computational fluid dynamics. Chem. Eng. J. 96 (1–3), 81–98. https://doi.org/10.1016/j.cej.2003.08.025.

Wang, G., Dong, M., Wang, Z., et al., 2022. Removing cuttings from inclined and horizontal wells: numerical analysis of the required drilling fluid rheology and flow rate. J. Nat. Gas Sci. Eng. 102, 104544. https://doi.org/10.1016/j.jngse.2022.104544.

Wang, H.G., Liu, X.S., Li, H.Q., et al., 1995. An experimental study of transport of drilling cutting in a horizontal well. Acta Petrol. Sin. 16 (4), 125–132. https://

doi.org/10.7623/syxb199504018.
Wang, Z.M., Long, Z.H., 2010. Study on three-layer unsteady model of cuttings transport for extended-reach well. J. Petrol. Sci. Eng. 73 (1–2), 171–180. https://doi.org/10.1016/j.petrol.2010.05.020.
Yan, T., Qu, J.Y., Sun, X.F., et al., 2020. Numerical investigation on horizontal wellbore hole cleaning with a four-lobed drill pipe using CFD-DEM method. Powder Technol. 375, 249–261. https://doi.org/10.1016/j.powtec.2020.07.103.
Yan, T., Qu, J.Y., Sun, X.F., et al., 2019. Investigation on horizontal and deviated wellbore cleanout by hole cleaning device using CFD approach. Enegry Sci. Eng. 7 (4), 1292–1305. https://doi.org/10.1002/ese3.346.
Yan, T., Wang, K., Sun, X.F., et al., 2014. State-of-the-art hole-cleaning techniques in complex structure wells. Recent Pat. Eng. 8 (1), 50–57. https://doi.org/10.1016/j.rser.2014.05.047.
Zhou, J.W., Du, C.L., Ma, Z.L., 2018. Influence of swirling intensity on lump coal particle pickup velocity in pneumatic conveying. Powder Technol. 339, 470–478. https://doi.org/10.1016/j.powtec.2018.08.043.